DEPTH-SENSITIVE ANALYSIS OF FLUORINE ON LUNAR SAMPLE SURFACES AND IN CARBONACEOUS CHONDRITES BY A NUCLEAR RESONANT REACTION TECHNIQUE

Thesis by

Richard Henry Goldberg

In Partial Fulfillment of the Requirements

for the Degree of

Doctor of Philosophy

California Institute of Technology

Pasadena, California

1976

(Submitted May 27, 1976)

ACKNOWLEDGEMENTS

I wish to express my sincere appreciation to Professor Thomas A. Tombrello, whose thoughtful advice, guidance, and help were indispensable during the course of this work. Many thanks go to Professor Donald S. Burnett for his aid and collaboration in all phases of this research.

I would like to thank all the members of the Kellogg Radiation Laboratory for support, assistance, and encouragement throughout my course of study. Particular thanks go to members of the Kellogg poker group and ghetto for both technical aid and much needed moral support.

I appreciate the help of Professors L. Silver and S. Epstein in procurement and handling of lunar samples used in this study. I am grateful for the financial support given to me by Caltech through research and teaching assistantships. This research was sponsored by National Aeronautics and Space Administration grant NGR-05-002-333 and National Science Foundation grant PHY 76-02724.

Last but not least, I thank Ms. Sharon Hage for her excellent work in typing this thesis.

And to Linda, Mom, and Dad - Courage! On les aura les boches!

ABSTRACT

The nuclear resonant reaction $^{19}F(p,\alpha\gamma)^{16}O$ has been used to perform depth-sensitive analyses of fluorine in lunar samples and carbonaceous chondrites. The resonance at 0.83 MeV (center-of-mass) in this reaction is utilized to study fluorine surface films, with particular interest paid to the outer micron of Apollo 15 green glass, Apollo 17 orange glass, and lunar vesicular basalts. These results are distinguished from terrestrial contamination, and are discussed in terms of a volcanic origin for the samples of interest. Measurements of fluorine in carbonaceous chondrites are used to better define the solar system fluorine abundance. A technique for measurement of carbon on solid surfaces with applications to direct quantitative analysis of implanted solar wind carbon in lunar samples is described.

TABLE OF CONTENTS

TABLE OF CONTENTS (Continued)

I. INTRODUCTION

For a number of years, nuclear resonant reactions have been used by experimenters to probe solid media for various light elements. Particular interest has been paid to properties of surfaces and surface-related phenomena, such as oxidation, diffusion, ion implantation, radiation damage, and atomic sputtering. This work applies nuclear techniques to the specific problems and properties associated with the outer micron of lunar materials, in order to answer questions pertaining to the interaction of the lunar surface with solar wind ions, lunar volcanism, and micrometeorite impact. Each of these processes affect the physical and chemical properties in a particular way and are specific to certain elemental species: solar wind (H, He, C, N, O, noble gases);volcanic events (S, halogens, volatile metals, Pb); meteoritic impacts (C, Fe, Ni, Ir).

The motivation for this study was provided by early work in the lunar science program on the measurement of fluorine in lunar samples. The element fluorine is a minor element in the solar wind (10^{-7} of the abundance of solar wind protons, Withbroe, 1971) and, although not depleted in lunar rock and meteorites, is not a major element either. Its prominence in terrestrial volcanic vapors would lead to the belief that fluorine might be associated with lunar volcanic events. Results from Surveyor VII (Patterson et al., 1970) indicated the possible presence of F-rich surface coatings on a lunar rock in the Tycho region, yet no such conclusions could be reached from early bulk analyses of lunar rock and soil (Reed and Jovanovic, 1973). Data

from meteoritic data had been largely inconsistent, and were high in comparison to these bulk analyses. Therefore, a depth-sensitive technique of high precision would be necessary to resolve these problems and probe the nature and abundance of fluorine in both lunar and meteoritic material.

A large portion of the work associated with the lunar science program has involved investigation of particle bombardment of the lunar surface, and the contribution of solar wind and cosmic ray atomic species to lunar surface chemistry. One such element is carbon, which, while indigenously low in lunar abundance, is a significant contributor to solar wind and meteoritic composition. It would be expected that carbon would exhibit the same inverse grain size, i.e., surface correlated, dependence that rare gases (He, Ne, Ar, Kr, Xe) do (Eberhardt et al., 1970). In fact, DesMarais et al. (1973) find a more complicated size fractionation, which clouds the interpretation of the nature and source of lunar sample carbon. Although they report surface correlated carbon in < 100 μm diameter soil particles, carbon-rich aggregates are more abundant in larger size fractions, and a volume correlated carbon component is indicated. Surface exposure is coupled with micrometeorite impacts in redistributing carbon into agglutinates, glasses, and other impact materials.

A better understanding of the problems and processes associated with lunar carbon chemistry would be achieved if a direct measurement of surface and volume lunar sample carbon could be made. Estimates of solar wind surface carbon, obtained indirectly by calculation from chemical measurements (Epstein and Taylor, 1975; Bibring et al., 1975)

are highly variable, ranging from 10^{14} to 1×10^{15} atoms/cm^2. A reliable measurement of surface carbon has not yet been made; Stauber et al. (1973), detecting protons from the $^{12}C(d,p)$ reaction, were compromised by hydrocarbon buildup in unsuitable vacuum conditions. Thus a nondestructive technique for measuring carbon concentration versus depth in lunar samples would be useful.

The nuclear reaction $^{19}F(p,\alpha\gamma)^{16}O$ is used for measuring fluorine on the surfaces of lunar samples; $^{12}C(d,p_0)^{13}C$ is the reaction chosen for carbon measurement (Table 1). In Chapter II of this thesis the experimental methods and special apparatus employed in these studies are described. Chapter III discusses measurements of fluorine in carbonaceous chondrites to define a meteoritic abundance. Chapter IV describes the experimental results of probing lunar samples for fluorine, and the various problems associated in sample contamination. Chapter V includes discussion of these results and conclusions drawn concerning fluorine chemistry on the moon. The experimental results of Chapters III (Goldberg et al., 1974) and IV (Leich et al., 1974; Goldberg et al., 1975, 1976) have been described elsewhere.

II. EXPERIMENTAL METHODS

Experimental Method - Fluorine

The technique of employing a resonant nuclear reaction to measure depth profiles or surface concentrations of trace ions in material media has been used many times before (see, for example, Phillips and Read, 1963; Ollerhead et al., 1966; Amsel et al., 1968). The reaction $^{19}F(p, \alpha\gamma)^{16}O$, in particular, has been utilized to measure both fluorine and hydrogen content in a variety of solids (Möller and Starfelt, 1967; Padawer, 1970; Leich and Tombrello, 1973), and is so well known as to be used for a beam energy calibration standard (Marion, 1966; Beckner et al., 1961).

The resonance in the $^{19}F + p$ system which is used in this study occurs at a center-of-mass energy of 0.83 MeV, which corresponds to an incident proton energy of 0.872 MeV (Marion, 1966) when measuring fluorine concentration depth profiles. The reaction has a peak total cross section of 540 millibarns, with a full-width at half-maximum of 4.7 keV. The resonance is well isolated, the off-resonant cross section being negligible. The reaction product ^{16}O nucleus is left in one of three excited states, at 6.131, 6.919, and 7.119 MeV. All three states decay promptly and directly to the ground state with greater than 99% probability via gamma ray emission (Ajzenberg-Selove, 1971).

Since the off-resonant yield is negligible (less than 20 mb) in comparison to the resonant gamma ray production rate, the sample depth being probed is uniquely determined by the incident proton energy.

At a proton beam energy of 872 keV, ^{19}F nuclei on the surface of the target only will contribute to the gamma ray yield, since protons penetrating the samples would be below resonance energy as they lose energy. For a bombarding energy E_0 slightly greater than E_R, the protons would lose energy until, at a depth X_R, their energy would equal E_R, where the copious production of gamma rays would take place. Thus, the gamma ray yield due to a proton beam of energy E_0 originates from a sample depth $X_R = (E_0 - E_R)/(-dE/dX)$, where dE/dX is the energy loss rate per unit path length in the sample.

The relationship between the concentration of fluorine atoms and measured gamma ray yield involves a number of other factors, as explained in Appendix I. Equation A1 gives the relation between the gamma ray yield and the concentration of ^{19}F at depth X_R, energy loss in the medium, and the resonance width Γ. This treatment is valid up to a proton energy where another $^{19}F(p, \alpha\gamma)^{16}O$ resonance producing the same γ-rays occurs: 0.935 MeV, corresponding to a depth limit of 1.2 μm. If one goes to higher bombarding energies (i.e., greater depths), the yield from this second resonance must be subtracted. However, since the significant region of interest in the samples of this study is the outermost micron, the unfolding procedure has not been utilized in this work.

The benefits of this type of profiling are severalfold. One, the sensitivity of this technique, as determined by the cross section and isolation of the resonance, as well as background due to other reactions, is excellent. Competing reactions with γ-ray yields in

the energy region in question are at a level of 10-15 counts/μC proton beam exposure. This is derived from experimental sampling of quartz glass and other typical host materials. A 2σ statistical counting uncertainty of ±20% over the step of the resonant yield corresponds to 10-15 ppm F. Typical thick target yield uncertainties are derived from the standard statistical counting errors, and for a typical total charge collected of 90 μC per sample, ± 8 ppm is quoted.

The depth resolution achieved with this procedure is principally derived from the width Γ of the resonance, (4.7 keV in the incident proton channel). As stated by Möller and Starfelt (1967), the depth resolution ΔX due to the resonance width is $\Gamma/2(-dE/dX)$, which for most materials studied is 0.05 micron at the surface of the samples. The spread in beam energy (~ 1 keV) and straggling at sample depths must be folded in with the resonance width to account for the full depth resolution,

$$(\Delta X)^2 = (\Delta X_{E\ \text{proton}})^2 + (\Delta X_{\Gamma})^2 + (\Delta X_{\text{straggle}})^2 \ . \qquad (1)$$

Only the straggling is depth dependent, and causes a resolution versus depth relation shown in Figure 1, showing the 0.05 micron resolution at the surface degrading to 0.10 micron at a depth of 1 micron.

Depth profiles are obtained using a proton beam from the CIT-ONR tandem accelerator, with the samples in an ultra-high vacuum scattering chamber (see Experimental Apparatus section). Data points are taken at 6 keV intervals from 0.850 MeV to 0.930 MeV, with intermediate points established if the F depth profile shape needed better definition.

Standard data points are obtained from 6 microcoulomb proton exposures at beam currents of 30 nA with the beam being magnetically deflected from targets after the completion of the prescribed charge integration. This low current at low bombarding energy produces a sample heating of 25 milliwatts into a 2 × 2 millimeter beam spot (defined by upstream slits). Therefore, the volatile elements studied are not diffused through the sample or driven off the surface.

Calibration of depth versus beam energy is calculated from known energy loss tables (Northcliffe and Schilling, 1970)

$$X_R = (E_0 - E_R)/(-dE/dX). \qquad (2)$$

This simple relation is a consequence of the small energy region over which this experiment is done, so that the energy loss can be assumed constant. Conversion of gamma ray counts to F concentration is made by the ratio obtained for a standard target, 300 $\mu g/cm^2$ CaF_2 (reagent grade) evaporated onto a Ta backing. Further details of this experimental procedure and the equipment involved will be given in the Experimental Apparatus section and appendices to follow.

Experimental Procedure - Carbon

The reaction $^{12}C(d, p_0)$ offers a different approach to depth profiling by nuclear reactions than had been used before in this work, since it involves detection of charged particles rather than high energy gamma rays. The reaction occurs with a Q-value of 2.722 MeV, advantageous from the standpoint of being well above elastic scattering and oxygen target reactions (Table I). Beam energy versus target depth and particle yield versus concentration conversions are complicated by the fact that energy loss and straggling had to be considered not only in the entrance channel but also in the exit channel. Also, the detection system, data acquisition and analysis are different. Since this is not a resonant reaction, rather than obtaining depth profiles by varying the incident beam energy, the concentration versus depth dependence would be determined from the proton energy spectrum obtained at a particular deuteron bombardment energy. Thus it had to be determined what bombardment energy would be most advantageous in terms of particle yield, sample heating, energy loss and straggling, and depth dependence of particle spectrum.

Back angles (near 180°) were chosen for the measurements for the following reasons: first, at back angle the beam penetration to a depth x and path length of reaction particles exiting the sample are minimized. Second, angular distributions for this reaction measured by Kashy et al. (1960) show that the (d, p) cross sections at all deuteron energies increase dramatically with increased θ. Therefore, both depth resolution and sensitivity are enhanced at back angles.

After preliminary experimental data were taken for thin carbon films in a large scattering chamber, a silicon surface barrier detector was mounted in the ultra-high vacuum target chamber at a lab angle of 160° (see Experimental Apparatus section). A differential cross section curve at 160° (lab) is shown in Figure 2, encompassing deuteron energies of 0.8 to 1.5 MeV, which agrees with the data of Kashy et al. (1960) taken at θ_{lab} = 158.4°. Absolute cross section determinations were not attempted as part of this work, since surface and volume concentrations of carbon can be derived from ratios to known thin and thick carbon standards. The data points in Figure 2 are integrated count rates over the width of the thin target yield curve, shown on a sample thin target spectrum of Figure 3, for an 11.2 $\mu g/cm^2$ carbon layer on a fused silica backing. The full width at half maximum of 9.4 channels at a deuteron bombardment energy of 1.07 MeV corresponds to 53 keV, which converts to one micron thickness.

A thick target of natural calcite (Hilton deposit) $CaCO_3$ was chosen as a calibration standard because of its high carbon content (12.00% stoichiometrically) and its energy loss, which is comparable to that of lunar samples (see Appendix II). As can be seen from the various thick target spectra of Figure 4, at energies of 1.10 MeV and higher, the proton spectrum is complicated by the shape of the cross section curve, and deconvolution into thin and thick components for a sample would be difficult. At E_d = 1.07 MeV, the thick yield is flat to ± 5%, and to a depth of 2.5 μm, thus affording maximum depth probe with a simple spectrum. In addition, the low bombarding energy limits beam heating of samples and radiation levels, and is sufficiently down

on the coulomb barrier for heavy elements as to minimize $^{28}Si(d, p)$ background. As E_d increases, the yield of the various proton groups from $^{28}Si(d, p)$ increases rapidly, and is the major source of background under the $^{12}C(d, p_0)$ particle yield spectrum.

Figure 5 shows a schematic of how proton energy varies with depth in a sample prior to penetrating the detector entrance foil. An additional energy loss occurs in the foil, so that (see Appendix III)

$$E_p(\Delta X) = E_{p_{max}} + 0.6\,(E_d - E_{d_0}) + \Delta X \sec 20^\circ\,(dE/dX)_{p.s.}$$

$$+ (dE/dX)_{p.f.} \times t_f \ .$$

(for E_d = 1.07 MeV, $E_{p_{max}}$ = 3.002 MeV). The proton energy resolution in the spectra is a combination of several factors as shown in Figure 3, $(\Delta E)^2 = (\Delta E_{det.})^2 + (\Delta E_{noise})^2 + (\Delta E_{samp.\ strag.})^2 + (\Delta E_{foil\ strag.})^2$.

Since the energy resolution of the protons is degraded by a number of factors so as to be no better than ± 0.5 μm, deconvolution of the proton yield into a depth profile is somewhat suspect. What is useful in terms of carbon concentration versus depth is primarily a surface component in atoms/cm^2 and a volume component in μg C/g sample. This can be obtained by a three component linear regression analysis of a sample spectrum, i.e.,

$$f(E) = a_0 + a_1 g_1(E) + a_2 g_2(E) \ ,$$

where a_0 is a background from other particle reactions, $g_1(E)$ is the experimental thin target spectrum (Figure 3), and $g_2(E)$ the experimental thick target spectrum (Figure 4). Thus a_0 = background average

count level from silicate target,

$$a_1 = \frac{\text{surface C concentration (atoms/cm}^2\text{)}}{11.2\ \mu g/cm^2\ C}$$

and

$$a_2 = \frac{\text{volume C concentration (}\mu gC/g\text{ sample)}}{0.12 \times 10^6\ \mu gC/g\text{ sample}} .$$

Since levels of carbon on surfaces of lunar samples are expected to be 10^{14}-10^{16} atoms/cm^2, it must be established that "blank" samples such as terrestrial fused quartz contain low enough surface C enhancements to guarantee that the source of measured lunar sample carbon is truly lunar. Preliminary measurements on such blanks show fairly large surface C films, on the order of 10^{15} atoms/cm^2. Various cleaning procedures, including perchloric acid etching and ultra-high vacuum bakeout to 300 °C failed to remove these layers entirely (minimum surface C = 4×10^{14} atoms/cm^2), and even prolonged residence in the target chamber also increased surface C levels. This was also the case for rock 65315, which was freshly split in the sample handling glove box (Appendix IV), and carbon levels on these rock surfaces were within 20% of other freshly exposed terrestrial samples (Figure 6).

Two samples from lunar rock chip 64455,33 were stored in the dry nitrogen glove box (Appendix IV) and would therefore have minimum atmospheric exposure. The solar wind exposed exterior sample had a surface carbon layer of 6.7×10^{15} atoms/cm^2; the rock interior sample 4.5×10^{15} atoms C/cm^2. The corresponding concentrations averaged over 1-3 micron depth were 280 ppm and 212 ppm, respectively. Therefore,

this technique can establish an upper limit for solar wind implanted carbon of 2.2×10^{15} atoms/cm^2.

The carbon levels do not correlate with H concentrations on the sample surfaces, indicating that the source of the contaminant is not hydrocarbons from cleaning solutions or beam line pump oils. Rather, it is assumed that all samples adsorb a monolayer of CO or CO_2 from the atmosphere. Since the dry nitrogen used to vent and flush the target chamber is passed through a liquid nitrogen cold trap, carbon monoxide is the more likely candidate. It is probable that the samples stored in the dry nitrogen glove box and security safe are unsuitable for this experiment, and only an Apollo 17 core tube sample stored in a vacuum might be sufficiently clean. This contamination would not affect bulk carbon results (for example, Epstein and Taylor, 1975; DesMarais et al., 1975), but may account for the inverse grain size distribution results. The findings of Simoneit et al. (1976) of large increases in vacuum pyrolysis low temperature (i.e., surface located) gas release of CO and CO_2 with prolonged atmospheric exposure agree with the findings mentioned above, and recommend the development of special sample handling procedures before the Apollo 17 core sample is opened.

Experimental Apparatus

The experimental program undertaken in this research has several important components which are unique to the problem of measuring near-surface atoms in solid samples. Since both lunar and meteoritic material have long been exposed to large particle and radiation fluxes, the resultant damage makes them highly absorptive for gaseous contaminants, particularly H_2O, CO, and CO_2. In addition, the high sensitivity which this work attempts necessitates maintenance of ultra-clean environment for the samples. Although this may not be a requirement for the fluorine measurements, for the sake of the carbon and hydrogen measurements a versatile ultra-high vacuum system was constructed.

The pumping available in the beam line of the tandem accelerator is by oil diffusion pumps, reaching 1×10^{-6} torr pressure, up to the entrance to the ultra-high vacuum chamber (Figure 7). In order to isolate the clean system from the vapor contaminants present in the upstream beam pipe, an in-line liquid nitrogen trap is inserted. A 40 cm long, 1/2" diameter tube surrounded by a liquid nitrogen reservoir allows maintenance of pressure differential between the two pump stations and condenses oil vapor which would drift into the target chamber. Normal bombardment of targets in an oil diffusion pumped system produces coatings of cracked carbon and polymerized hydrocarbons; thus, measurements of carbon and hydrogen could not be done under such conditions.

The ultra-high vacuum system is constructed from a stainless steel 6 inch diameter (nominal) tee with several 2 inch ports, mated

to an Ion Equipment Corporation Model CV-500 combination stainless steel getter-ion sublimation pump. The getter-type ion pumps, along with the zeolite molecular sieve sorption roughing pump do not produce vapor during pumping (they are sealed from the atmosphere), and therefore are "clean". Low vapor pressure materials are used throughout the system, so that the base pressure achieved is $\leq 10^{-10}$ torr, the limit of reading the ion pump current.

Targets are held within the vacuum system in aluminum holders, two horizontal rows of six 5/8 inch diameter holes 0.640 inch apart, parallel to the beam axis. They are connected to an aluminum buss on the end of a 1/2 inch diameter rod of a Huntington VF-172 vacuum manipulator. Theta manipulation (about the vertical axis) is accomplished by magnetic coupling to exterior permanent magnets; vertical target shift is along a one inch travel micrometer feed. The target wheel, insulated from the buss attachment to the manipulator with quartz glass spacers, is electrically connected by copper wire to an I.E.C. FET-8 8 pin feedthrough, strung with glass and ceramic beads to insulate from the grounded walls of the vacuum system.

Since the system components are stainless steel, aluminum, copper, glass, and ceramic, and all seals are copper gasketed stainless steel knife edge seals, the entire vacuum system is bakeable to 300 °C. This allows quick (12-36 hour) pumpdown and low base pressure.

There are two detection systems employed in these experiments--a gamma ray detector and charged particle detector with associated electronic hardware. The investigation of fluorine concentrations in

lunar and meteoritic samples requires an efficient gamma ray detector, since the sensitivity desired is in the ppm range. Therefore, a 3" × 3" NaI(Tl) scintillation crystal mounted directly onto a photomultiplier tube is used. The maximum count rate of approximately 10^4 counts per second allows the use of the slower NaI(Tl) detector, since recovery time is not crucial. A Caltech-made preamplifier is connected to the phototube, and in turn AC-coupled to the input of an Ortec Model 410 linear amplifier. This amplification system is found to be well-suited to the noise level, count rate, and pulse shaping needs and characteristics of the experiment.

The pulses are subsequently analyzed by a multichannel analyzer to obtain a gamma ray energy spectrum; two analyzers have been used in this work. The bulk of the experimental data has been processed by a Nuclear Data Corporation Model 4420 16K-word memory analyzer, subdivided into 512 channel groups. Also used was a 400 word RIDL (24-2), divided in two 200 channel groups.

As stated in the previous chapter, the detection system is designed to count three principal gamma rays, of energies 6.131, 6.919, and 7.119 MeV. Since the incident proton energy is too low to excite heavy atoms and other proton induced yields are small, the counting window over which the gamma events are integrated can include full energy peaks, single and double escape peaks, and a large fraction of Compton scatter events created within the NaI(Tl) scintillation crystal. A sample gamma-ray spectrum from a standard CaF_2 target (Appendix II) is shown in Figure 8, with the limits of integration set at 3.6 to 7.2 MeV.

An Ortec 100 mm^2, 500 micron thick, partially depleted, silicon surface barrier detector is mounted in the vacuum system for $^{12}C(d, p_0)$ analysis. This detector thickness is sufficient to stop 8 MeV protons, which eliminates foldback effects from high energy protons originating from $^{28}Si(d, p_n)$ reactions. It is held in a one inch I.D. aluminum holder, at a lab angle of 160° to the incident beam, 2 3/8" from the front face of the target. A 1/8" wide collimator provides a 3° acceptance angle of scattered particles, which corresponds to ± 5 keV for $^{12}C(d, p_0)$ protons. A 0.0005 inch thick (3.43 mg/cm^2) aluminum foil is placed directly in front of the detector to stop elastic scattered deuterons, and is sufficient to stop elastic protons from the $^{19}F(p, \alpha\gamma)$ experiment. A schematic diagram of the target chamber and detectors is shown in Figure 8.

The detector is electrically connected by coaxial cable to the 8 pin electrical feedthrough. The external pin is directly connected by coaxial cable to a Canberra Model 808 charge-sensitive preamplifier.

Due to the high noise level of surface barrier detectors, a Tennelec TC200 linear amplifier is used in conjunction with the Canberra preamplifier. The amplified, shaped pulses are analyzed by the Nuclear Data 4420 multichannel analyzer in 1024 groups. A spectrum taken at 1.07 MeV deuteron energy on an 11.2 $\mu g/cm^2$ carbon foil on quartz glass backing is shown in Figure 3 (gain is 6 keV/channel).

Since the detector is exposed only to the 10^{-10} torr vacuum of the target chamber or to dry nitrogen during target change (Appendix IV), there is a difficulty encountered in depletion of adsorbed oxygen on

the detector front surface. This eventually causes severe loss in resolution and microplasma breakdown, which can be corrected by exposure to atmosphere for a sustained period. Since this is inconvenient for the purpose of these experiments, an alternative is to keep the detector nominally biased (+20 volts) at all times, which maintains the surface oxide layer.

III. FLUORINE IN CARBONACEOUS CHONDRITES

In conjunction with the long term study of the source and magnitude of fluorine concentrations in lunar samples, a series of measurements was carried out on a variety of carbonaceous chondritic meteorites. These meteorites have long been believed to most closely resemble the average elemental solar system concentration (Anders, 1964; Suess and Urey, 1956). Thus, a detailed examination of the fluorine concentration in the carbonaceous chondrites would give a reliable indication of the true solar system fluorine abundance. Previous work on this problem (Fisher, 1963; Reed, 1964; Greenland and Lovering, 1965) had given a large range of meteoritic concentrations, although the number of samples looked at was small. All measurements gave high fluorine abundances in light of cosmic ray abundance data (see, for example, Teegarden et al., 1973).

Thus it was deemed important to better define the fluorine abundance in carbonaceous chondrites, and the technique of using the reaction $^{19}F(p, \alpha\gamma)^{16}O$ afforded a method with good sensitivity and reliability. As seen from the measurements of fluorine on lunar sample surfaces, since only the outer micron is sampled, the method is greatly susceptible to contamination and non-uniformity in samples. The handling and preparation of meteorites thus become important in terms of developing a consistent and clean method of sample manipulation for measuring fluorine concentrations.

The experimental method used in F analysis of carbonaceous chondrites has been described earlier in sections on Experimental Procedure

and Apparatus. A typical gamma ray counts versus proton energy plot is shown in Figure 9, which is the raw data curve for two samples of the Murchison meteorite. The jump in the yield versus energy at E_p = 872 keV indicates it is fluorine that is being measured, since there are no other competing reactions of large magnitude at this energy. The distribution of fluorine is fairly flat with depth, and shows no sign of a contaminant, which would be seen in the form of a surface peak. This is an important consideration, since the method probes a small volume of the sample, i.e., 2 mm × 2 mm × 1 μm. Surface irregularities such as chondrules (high temperature minerals and metal grains) found in these samples could affect the results greatly, and thus two checks on consistency were performed.

First, a number of assays on the same meteorite, Murchison, (see Table 2) were done on different chips and sawed fragments, thus sampling a larger volume of the sample. Chips were taken by chiseling a fragment of the meteorite into roughly 10 mm × 10 mm × 5 mm pieces; sawing with a diamond wafering blade of a low-speed rock saw and a diamond impregnated copper wire saw produced slices of the same size. The table demonstrates the interconsistency of the Murchison results, which average 75 ± 13 ppm F. These "solid" samples measure the effects of handling procedures, but no discernible altering of the fluorine depth profiles or content was observed.

In all cases, the profiles were constant with depth, the reported fluorine concentration being obtained from a below resonance average counting rate subtracted from an above resonance average, and comparing

to a known standard (Appendix II). The statistics quoted are governed by the count rate, total integrated charge, background, and number of data points taken, and are generalized to be ± 8%. Irradiation of the samples was observed optically due to meteorite fluorescence under proton bombardment, so that an accurate appraisal of beam position on the samples was easily accomplished.

In order to simulate a bulk analysis of homogenized meteoritic samples, a number of chips were crushed to < 75 μm grain size, and the resultant powder was pressed into 3 mm diameter recesses in 13 mm diameter stainless steel discs (Goldberg et al., 1974). This crushing process yielded a relatively homogeneous meteorite powder, which when measured for fluorine content exhibited the concentrations shown on Table 2. The beam was situated visually as with the solid samples, uniformly illuminating the fluorescing powder.

The number of different crushed meteorites run allowed comparison of the different types of carbonaceous chondrites, since there is disagreement as to which represents solar system abundance more closely (Suess and Urey, 1956). Since the suite of crushed samples contains a larger number of CII carbonaceous chondrites than either CI or CIII, the fluorine abundance of CII can be stated with the greatest degree of confidence. The number 755 atoms F/10^6 atoms Si is arrived at, versus 1009 for CI and 559 for CIII, from a small sampling. A generalization of abundances of elements of varying degree of volatility (Larimer and Anders, 1967) gives the ratio for CI:CII:CIII meteorites as 1:0.6:0.3. The crushed meteorite results show a ratio of 1:0.75:0.55, in fairly good agreement; the conformance is better for fluorine

(Larimer and Anders, 1967), quoted as 1:0.69:0.38. However, the absolute abundances established in this work are lower than the Larimer and Anders number by a factor of 3.

Thus, the results presented here are in agreement with previous evaluations of fluorine ratios between the carbonaceous chondrite species, and the concept of undepleted and depleted component mixing (Larimer and Anders, 1967). However, they do suggest a lower solar system abundance for fluorine than that found by Fisher (1963) and Reed (1964).

IV. FLUORINE IN LUNAR SAMPLES - EXPERIMENTAL RESULTS

Measurements by other experimenters of halogens and halides in lunar samples (Reed and Jovanovic, 1973) and on sample surfaces (Meyer et al., 1975; McKay et al., 1973) indicate that fluorine is definitely not a depleted element, and possibly is surface enhanced in some cases. Although bulk analyses of rocks and soils showed fluorine in abundances not higher than 100 ppm (Jovanovic and Reed, 1974), the Surveyor VII measurement on the lunar surface by a technique sensitive to sample surface layers showed up to 3000 ppm F (Patterson et al., 1970). In light of observation of high halogen content in terrestrial volcanic gases (Naughton et al., 1972), it would be important to ascertain the nature and abundance of fluorine in lunar soils and rocks. The experimental nuclear resonant reaction technique, as described earlier, allows precise, accurate measurements of fluorine concentration depth profiles in the outer micron of lunar samples.

Preliminary Findings

The preliminary assays of a number of Apollo 16 rocks and coarse fines were encouraging, as Table 3 shows. The large surface enhancements found on a number of rock chips and soil fragments seemed to demonstrate large F deposits; the fact that lunar exterior samples generally were more enriched in fluorine was also evidence of lunar deposition on surfaces. It became critical to ascertain the exact exposure and handling history of the samples in question, since the experimental method would be unable to differentiate lunar F in the

form of halides from terrestrial contaminant F, as from Teflon and Freon. These materials were used extensively in the packaging of samples during Apollo missions and at the Lunar Curatorial Facility in Houston, Texas, which prepared and sent out all sample allocations. If indeed the heat sealing and abrading of rock and soil in the Teflon sample bags resulted in deposits of Teflon on the lunar samples, the preliminary results would be hopelessly clouded. In spite of the contamination problem, several features of the data taken from early samples were possible indications of lunar fluorine.

First, high concentrations of F were observed to a depth of one micron (Figure 10), particularly on samples 66044,8 and 75075,2. The F levels below 0.2 μm on these depth profiles are relatively constant, as opposed to hydrogen profiles of H_2O contamination, which show no penetration below a 0.1 micron depth (Leich et al., 1974). In addition, the fact that exterior surfaces (those exposed to solar particle bombardment) consistently showed higher F contents than interior surfaces, although Teflon exposure would be equal, seemed to indicate that perhaps there were real lunar fluorine enhancements, though the extent of these enhancements was shrouded by the possibility of contamination.

Several experimental tests were performed to determine the effect of packaging samples in Teflon. First, the coarse fine anorthosite 66044,8, which showed the largest F content of any sample measured (Table 3), was split in order to expose a fresh interior surface. Since the original sample had been transported in Teflon, the clean, fresh interior would indicate whether or not the fluorine found in

66044,8 was indigenous to the sample or a contaminant. As seen in Figure 10, the interior surface contained less than 100 ppm F, consistent with bulk analyses of lunar material and with the measurements on other solar system material, namely the carbonaceous chondrites described in Chapter III. This definitely indicated sample 66044,8 was not fluorine rich, and the large concentrations found in the outer micron were suspect.

As a better measure of the contamination induced by Lunar Receiving Laboratory packaging, a controlled experiment was performed with terrestrial quartz glass. After establishing the fact that quartz discs chemically cleaned and vacuum baked (300°C) were fluorine free (< 20 ppm F, a 2σ upper limit), two discs were sent to the Lunar Receiving Laboratory for packaging in Teflon sample bags. The handling given these controls was identical to that for the samples previously measured. Analysis of these quartz discs, the results of which are shown in Figure 11, demonstrated the bagging contaminant. A substantial surface fluorine enhancement is observed for the packaged sample, which extends to the 1 μm depth limit of the experimental technique. This result, although of a much smaller magnitude than the concentration found on the 66044 and 75075 chips, nevertheless proved the packaging introduced large fluorine surface contaminants. The fact that the quartz samples were lower in F than the lunar samples can be explained by surface smoothness (i.e., less abrasion and adhesion to surfaces), length of time in bags, outgassing of bags in the vacuum of the lunar environment, vibration during Apollo missions and splashdown, etc.

The 1 μm depth (or thickness) of the contaminant fluorine indicates a statistical size and coverage distribution of Teflon particles which can account for the lunar sample results. The problem of identifying true lunar fluorine and measurement of depth distributions became that of finding samples clean enough to eliminate the possibility of contamination as a source. It should be noted that the Teflon found on sample surfaces would not affect the measurements of bulk sample concentrations.

Prime candidates for F depth probe in terms of lunar exposure to halogen-rich vapors and minimal contaminant exposure are vesicle linings in basaltic rocks, and volcanic glasses which show sublimate coatings (Meyer et al., 1975). Evidence for volcanic emanation surface coatings on Apollo 15 green glass soils and Apollo 17 orange soils have been found in ion and electron microprobe studies (Jovanovic and Reed, 1974; Meyer and McKay, 1974) and in chemical leaching experiments (see, for example, Tera and Wasserburg, 1976; Jovanovic and Reed, 1974).

The first attempt to examine the nature of vesicular rocks was made on Apollo 17 rock 76215. This sample was brought back from the lunar surface in a Teflon bag; however, the vug 76215,32, a deep, crystalline-lined cavity, should have been shielded from contact with the Teflon. In contrast, the depth distribution of F was measured on a projecting knob of this rock, 76215,19, to indicate the effect of the bagging on a portion of the sample which would definitely be in contact with Teflon. The F depth distribution profile shown in Figure 12 displays the large amount of Teflon found on the knob surface, while

the vug is a factor of 10-15 lower in fluorine than the knob. If the observed fluorine were the result of lunar atmospheric deposition, there would be roughly 1/3 the fluorine as that on a flat surface owing to ballistic deposition into a hemispherical cavity (Goldberg et al., 1975), as opposed to the order of magnitude difference observed. If the source were the outgassing of the magma from which the rock cooled, the result should be a larger concentration on the vesicle lining from reaction with the vesicle-causing gas bubble. In addition, the similarity in profile shapes leads to the conclusion that the fluorine found in these rock chips must be a contaminant. The nature of this surface deposit could be either a thin film of adhering particles deposited during bag outgassing in the lunar vacuum, or from compression of the bag onto the sample during LM repressurization, or both. The F found on the vug could be lunar in origin, but the pristine vug surface might preferentially getter an atmosphere created by bag outgassing. The samples had been ultrasonically cleaned in methanol; thus, the surface coating is not a superficial adhesion.

Soil Breccias

The first samples obtained which were handled cleanly with respect to fluorine were two glass-coated soil breccia chips from soil sample 15012. Transported in a Sealed Environment Surface Container (SESC), these samples were never exposed to Teflon or other F-rich substances. The vacuum seal did not hold on this Apollo 15 SESC, but this may not be important for the purpose of this experimental work.

Fragment 15012,67 is an elliptical (3×5 mm) chip which is partially covered by vesicular brown glass. Lunar surface exposure is confirmed by microcraters observed under optical microscope examination; exposure to air was necessary in light of our eventual findings on this sample. The soil breccia surface of this chip was found to be impregnated with green glass spheres, up to 10% of the total sample surface area. 15012,63 is quite similar--a 3 mm × 5 mm triangular prism partially coated with vesicular brown glass. This coating covers two surfaces of the prism analyzed as "soil breccia", which again contains a large number of green glass spheres. A visual estimate of 40% (Goldberg et al., 1975) coverage by green glass was significant in terms of analysis of fluorine data on this sample.

The results of depth probes on the surfaces of the two 15012 breccias should be studied in terms of the two types of surfaces found--"glass" and "soil breccia". Since they are very different, they will be considered separately; all depth probe results are shown in Figure 13.

There is no evidence for surface F enhancement on either of the glass surfaces, which have uniform fluorine depth distributions of 120 ppm (, 63) and 70 ppm (, 67). These are consistent with Apollo 15 soil and basalt bulk analyses quoted previously (Reed and Jovanovic, 1973). Since the microimpact pits show lunar surface exposure, these are the only lunar exterior samples (except 64455 - Leich et al., 1974) which have not exhibited surface peaks. Not coincidentally, they are the only samples thus far in this study not returned from the lunar surface in Teflon bags. In light of the aforementioned results on 76215, the conclusion is again confirmed that samples assayed prior to 15012 were terrestrially contaminated. The Teflon deposited on the samples could have consisted of particles as big as one micron in size. The profile of 66044,8 (Figure 10) is not influenced by surface charging. An average concentration observed at the 0.5 micron depth of 700 ppm requires only 0.09% surface coverage of C_2F_4. Since ultrasonic cleaning leaves these contaminant layers unchanged, light surface adhesion is unlikely; heat-sealing of sample bags may bond Teflon particles to sample surfaces. This type of contamination would also affect proposed study of solar wind implanted carbon (see Chapter II).

As seen in Figure 13, the breccia surfaces of 15012 chips are entirely different, showing large surface peaks, and, somewhat surprisingly, substantial F concentrations at the one micron depth. The widths of the peaks are consistent with thin (< 0.1 micron) layers, limited by the full width at half maximum of the resonance used.

The levels at 0.4-1.0 micron deep are highly variable, particularly on sample 15012,67, but even after ultrasonic methanol rinse, the profile was basically unchanged. This cleaning resulted in the loss of at least one grain layer from the friable soil breccia surface, so that it is unlikely to be a surface contaminant that is observed. In addition, the glass surfaces showed no contaminant. As previously stated, the breccias contain significant fractions of green glass spheres, which are found to have large surface F enhancements (Meyer et al., 1975; Goldberg et al., 1976). Therefore, the interpretation attached to these profiles is that of a distribution of spheres which are partially covered by soil particles 0-1 μm in size, which explains both the variability and distribution with depth. The estimate of 10% coverage of the soil breccia surface would imply 3000 ppm surface concentrations for the 15012,67 green glass spheres; 10-20% is required below 0.4 μm to account for 500 ppm level at that depth. This is found to be consistent with subsequent results from Apollo 15 green glass measurements that are to be described below.

Apollo 15 Green Glass

Because of the results on the SESC samples, it was necessary for the purpose of these experiments to measure the F depth profiles of individual glass spheres similar to those found in the 15012 breccias. The volcanic origin of Apollo 15 green glass and Apollo 17 orange glass samples has been discussed at length (for example, Carusi et al., 1972; Meyer et al., 1975). Observations of volatile and sublimate ions on the surfaces of green glass samples point toward this conclusion. In particular, F and Cl enhancements associated with volatile metals (Zn, Cu, Ga, Pb) have been found.

The sample first examined in this vein is 15427,39, returned from the moon as part of a 5 gram green glass clod 15427,7 which was estimated to be 80% green glass. No lunar exterior was observed on this larger sample, probably due to its friable nature (P. Butler, private communication). This, and the fact that sample 39 was a central part of a disaggregated soil should make Teflon exposure negligible. The samples eventually run were grain separates handpicked under a binocular microscope. Two slightly different methods of mounting the samples were used, both utilizing stainless steel mesh, which is relatively fluorine free and vacuum bakeable (see Appendix IV for description).

Two size separates were prepared for depth profiling by dry sieving through meshes of 175 μm and 100 μm openings, and then separating by microscopic examination. Four samples were formulated from the original soil. (1) A $\geq$ 175 μm sample of handpicked, transparent

green glass spheres, as they came in the sample container. Two assays were made on this sample, one before cleaning and one after methanol ultrasonic rinse to remove dust particle coating. (2) A $\geq$ 175 μm sample, which represented the residue of the green glass after non-green glass fragments (i.e., brown glasses and crystalline fragments) were selected out. This sample contained primarily devitrified green glass, and was ultrasonically washed in methanol. (3) A 100 μm - 175 μm size fraction which also had brown glass, feldspar, pyroxene, etc. removed, and was ultrasonically cleaned in methanol. This sample contained primarily clear green glass particles. (4) A > 175 μm sample selected from the remainder of the soil particles, specifically brown glass fragments which were cleaned as the other samples were. Each of the four samples should be considered individually because of their particular characteristics.

The results of the depth probes of these four samples are shown in Figures 14 and 15, along with a "blank" sample composed of a screen and fluorine-free quartz disc, to indicate the contribution from the screen itself. The concentration scales are calculated under the assumption that the samples completely fill the beam spot area. Since this may not be entirely true for the > 175 micron samples, the concentrations shown may be conservative, but certainly by no more than a factor of 2. The 100-175 μm fraction did cover the collimated hole entirely, and the brown glass fragment yield was corrected for packing fraction by the $^{16}O(d,p)$ reaction technique (Appendix V), so the concentrations shown for these two samples are accurate.

The F concentration depth profile of the > 175 μm transparent green glass spheres, shown in Figures 14 and 15, show peaks of ~ 1000 ppm height, corresponding to 2.8×10^{15} atoms/cm^2 F surface concentration; Figure 14 shows the profile of the sample before cleaning, and Figure 15 displays the cleaned sample. The increase in peak height due to ultrasonic cleaning could be due to removal of superficially adhering dust particles masking the fluoride-coated green spheres, or could represent a slightly higher packing fraction of the sample after remounting. As indicated by the summary in Table 4, the surface concentration of fluorine on the Apollo 15 green glasses is variable, and the difference in F abundance after ultrasonic cleaning and remounting is most likely a reflection of that variability. The decrease in volume correlated F content due to washing, seen on Table 4, perhaps suggests the loss of F-rich small particles in the ultrafine 15427 material.

Sample 2 of the 15427,39 clod exhibited the highest surface concentration of fluorine yet observed, 6.0×10^{15} atoms/cm^2 (Figure 14). Since this sample was assembled after removal of transparent whole green spheres and non-green glass fragments, the result is somewhat surprising since there is a greater percentage of broken fragments in this sample. Sample 3, the green glass fraction from a smaller size range (100-175 microns) shows a lower surface F concentration (Figure 14, Table 4) than either of the > 175 micron samples. This may be a reflection of the greater proportion of broken spheres in the sample, and again demonstrates the great variability of fluorine content in the green glass.

In light of the preliminary results of F assays on lunar samples being dominated by Teflon contamination, the measurements of Sample 4 (brown glass and crystalline fragments from 15427,39) are important in confirming the "clean" history of the sample. It had been stated previously (Goldberg et al., 1975) that the 15427 sample was a clod which had no lunar exterior surface and was therefore free of fluorocarbon contamination. The possibility of contamination must be ruled out entirely if the experimental results are to be conclusive; some interior rock samples received from the curatorial facility, unexposed to Teflon, are apparently contaminated (see Vesicular Basalts section). The non-green glass particles provide a "blank" sample which has accompanied the glasses throughout their sampling history from the lunar surface to Caltech. Since they appear to be unexposed to the magmatic vapors responsible for green glass surface coatings, and mixed with the green glass during a subsequent impact event, the absence of any F surface peak on this sample would conclusively show the source of F deposits on the glasses is lunar. Such is the case, as shown by the "brown fragments" fluorine depth profile of Figure 15, which has no surface F enhancement.

Similar to these results, Lakatos and Heymann (1972) do not observe inverse grain size dependence in ^{4}He, ^{20}Ne and ^{36}Ar contents in green glass. This, and the high variability of the larger size F abundance can be understood in terms of a small fraction of F-rich spheres irregularly distributed throughout the green glass sample, in higher numbers in the larger spheres. An alternative explanation

(Reed, private communication) is that in the boiling of the lunar magma during a volcanic event, F is preferentially lost from smaller spheres. This, however, does not agree with the depth profile analysis which correlates high fluorine concentrations with surface deposits only, not with a volume component; the profiles are not indicative of a diffusion process. The depth variation of all green glass samples is that of a "thin" (less than a monolayer) deposit on a sphere of volume concentration 30-100 ppm; this is confirmed by the fact that the width of any profile equals that of the resonance. Small apparent increases in the widths of surface peaks can be ascribed to the curved surfaces of the glass particles and to differential electrostatic charging of the glass surfaces. This latter effect causes local deceleration of the beam and a resultant shift in beam energy to depth conversion, which if variable among the individual spheres would cause a spread in the peak width.

The "thin" layer finding is consistent with results of McKay et al. (1973) and Meyer et al. (1975), who discuss surface adhering F-rich mounds on glass spheres. These particles would be constrained to have sizes less than 0.1 micron to be consistent with the above mentioned depth profiles. In contrast to their results, data from Cavarretta et al. (1972) report qualitative agreement in bulk F analyses, but find no correlation with trace elements such as Zn, Ga and Pb, which are important in the Meyer et al. theory of halide sublimates. (This will be discussed at greater length later.) In addition, Cavarretta et al. report a factor of 6 less fluorine in devitrified

samples as compared to a green glass 15301 separate--opposite to these 15427 data. It is believed that this further points out the extreme variability of F-rich layers on green glass grains, and perhaps indicates that this is not an effect of the devitrification process.

Apollo 17 Orange Glass

The surface coatings of Apollo 17 orange soil particles provide an additional record of deposits of lunar volcanic vapors on lunar samples. The composition of these coatings includes enrichments in S (Grant et al., 1974; Butler and Meyer, 1976) and F (Goldberg et al., 1975) which indicates the vapor is lunar (as opposed to volatilized meteoritic material). A summary of observations of surface coatings and their constituent elements is given by Meyer et al. (1975). The measurements of fluorine continued with examination of the outer micron of Apollo 17 orange glass spheres in order to demonstrate the volcanic origin of these coatings.

Three samples of soil 74220 were received for this purpose: daughters 28 and 174 from L. Silver (Caltech), and daughter 235. Of these three, only 174 was packaged in the curatorial facility as a soil clod, contrary to what was originally believed (Goldberg et al., 1976). The advantage of receiving a sample as a clod, as opposed to a disaggregated collection of soil grains is that the center of the clod would be guaranteed to have been shielded from any contaminants. In addition, the rock and mineral fragments associated with the 28 and 235 samples of the 74220 soil may have compromised the ethnic purity of the sample during collection on the moon and would not be genetically related to the orange glass. Sample 174 is essentially all orange glass, whereas 28 and 235 contain substantial mineral and rock fragment components; the difference is established below.

In a manner similar to that of the green glass 15427, the 74220 samples were mechanically dry sieved through two stainless steel mesh sizes. Unlike the green glass, however, none of the orange glass remained in the > 175 micron sieve, and thus a > 100 micron size applies for all samples discussed. In all cases, the samples were ultrasonically rinsed in methanol to remove surface adhering dust particles. The samples probed for fluorine include the following: (1) 74220,28--an orange glass sample which included a large fraction of partially broken spheres in addition to the whole transparent glass balls. Feldspar, pyroxene and soil fragments were handpicked out of the sample under a binocular microscope. (2) 74220,235--a handpicked collection of orange glass spheres. (3) 74220,235--a handpicked collection of basalt fragments which served as a sample handling "blank" as for 15427 of the previous section. (4) 74220,174-- handpicked, whole, transparent orange glass particles. (5) 74220,174--the residue of the handpicked sample which contained broken and chipped orange glass fragments. The results of depth probes for fluorine on these samples are shown in Figures 16, 17, and 18, for samples 1, 2, and 3 through 5, respectively.

As seen from the figures, the experimental method used again readily distinguishes the surface layer of fluorine from the volume component. Deviations (i.e., slight broadening) of depth profiles from thin layers, equal to the resonance width, are caused by electrostatic charging of the individual glass beads and/or their curved surfaces. Again the profiles are consistent with their (< monolayer) films;

magnitudes of these surface F layers are indicated in Table 4. On the average, the F concentrations on the Apollo 17 orange soil surfaces are lower than the Apollo 15 green glasses. The most striking feature of the orange glass data is the factor of four difference between the whole 74220,174 orange beads and the broken orange glass fragments (Figure 18). This demonstrates the need to examine the original glass surfaces of these samples; the results agree qualitatively with the Meyer et al. (1975) findings that Zn is enhanced on whole sphere surfaces only, and not on interior or chipped surfaces.

The values quoted for surface and volume component of fluorine agree reasonably well with those quoted by Jovanovic and Reed (1974), who measure fluorine by water and/or pH 5 acid leaching of orange glasses. However, as described below, these leach results have not been reproduced when done on the above measured 74220 samples. An understanding of the chemistry of this surface coating will be attempted in the next chapter.

The results of measuring handpicked basalt fragments of 74220,235, shown on Figure 18, again prove that the sample was uncontaminated, and the source of orange glass surface F is lunar. This suggests a different origin for the basalt fragments from the orange spheres; the soil was probably mixed during an impact event subsequent to the formation of the orange glass.

Vesicular Basalts

Many lunar rocks, particularly volcanic basalts, display vesicularity which is caused by the boiling out of a vapor phase from the host magma, or by trapped gases of solar wind origin. The chemical composition of this vapor producing the bubbles is not well understood; a surface analysis of these vesicle linings would prove useful. If indeed this vapor were rich in fluorides as terrestrial volcanic gases are, a surface enhancement in F of the vesicle walls' fluorine profiles should be seen. Also important in terms of this concept is the bulk F concentration in the host rock, which presumably would have lost halogens during boiling and would be F depleted relative to the vesicles.

After several attempts at measuring the depth distributions of fluorine in vesicle linings (Preliminary Results section), it again became apparent that large contributions from Teflon sample packaging materials were obscuring any real lunar effects (Goldberg et al., 1975 and 1976). Special requests were made to the Lunar Curatorial Facility for freshly exposed, interior rock surfaces which had never come in contact with F bearing materials. A number of these samples were obtained and measured for fluorine in the ultra-high vacuum target chamber.

Sample 68815,229, although wrapped in aluminum foil, was double sealed in Teflon bags, and any results of experimental measurements would be suspect. The sample was a small (3×5×5 mm) chip taken from part of a vesicle lining--a concave, black, shiny surface with

two light inclusions, which, after binocular microscope examination, were concluded to be metallic or FeS droplets. The vesicle wall was found to be a network of crystalline grains, and seemed to be a good sample in terms of rock type and surface characteristics. Although the analysis for fluorine demonstrated a substantial enhancement over bulk rock values (~ 50 ppm), it was impossible to determine an accurate depth profile due to erratic electrostatic charging of the crystalline-glassy surface.

A large (3×1×1 cm) sawed rectangular sample 76215,79 was also exposed to Teflon, since it had been sawed by the Lunar Curatorial Facility with a Teflon coated blade. However, a large vug (crystalline lined cavity) on the north surface (as designated by Curatorial Facility documentation photographs) was freshly exposed by chipping; the sample was transported from Houston to Caltech in an aluminum can with inner Teflon liner. Attempts to depth probe the vesicle surfaces on the sawed areas showed the substantial Teflon deposits expected. In order to measure F on the north surface vesicle, the rock chip was sawed by a low-speed saw with diamond wafering blade, cooled by methanol spray. Measurements of saw blanks (F-free quartz sawed under identical conditions) showed no fluorine introduced by the slicing process. The vesicle of interest was found to have two large troilite (FeS) grains imbedded in a concave crystalline surface. As with sample 68815,229, the electrostatic charging of this material under proton beam bombardment made the depth profile nonreproducible and thus difficult to interpret. The fact that these two samples had possible

Teflon contamination discouraged further efforts to measure their fluorine profiles.

Two other vesicular basalts were examined with positive results: 15016,176 and 15556,94. Sample 15016 came to Caltech wrapped in aluminum foil, and had, according to Lunar Sample Allocation Program documentation, freshly exposed vesicular surfaces. Three of the surfaces of this 2×1×1 cm rectangular chip were sawed with a Teflon coated blade and stored in Teflon bags prior to chipping; therefore, these three were unsuitable for the needs of this experiment. The best surface in terms of vesicle size and intervesicular area (for sampling the host basalt for bulk rock fluorine) contained two freshly exposed cavities, as well as an intermediate surface that appeared to be freshly broken. Difficulties were encountered in confining the beam spot to a particular area of interest, and in confirming that the intervesicular rock was free of surface fluorine contamination.

Such was also the case for 15556,94 (a rounded 1.3 cm cube), and since the rock samples were sufficiently large and vesicle-rich, it was possible to expose fresh vesicle-bearing and clean basalt surfaces by sawing in the Caltech laboratory. The samples were sliced with the 0.3 mm thick diamond wafering blade (lubricated with methanol), along with a plagioclase crystal and fused silica rod to establish saw blanks. These blanks showed no surface F peaks ($< 0.03 \times 10^{15}$ atoms F/cm^2) and the sawing was confirmed as being a clean procedure. The SiO_2 rod was sawed in between each lunar rock slicing to monitor any possible F-rich deposits transferred to the samples or blanks; none

was found. From the sawing procedure, one fresh interior vesicle was exposed of sample 15016,176, two vesicles of sample 15556,94, and fresh, interior intervesicular basalt for each.

Figure 19 displays the two depth profiles of vesicles from rock 15556. Small, yet distinct, surface peaks are seen on both vesicles superimposed on a flat distribution above 0.4 micron depth (see Table 4). In comparison, Figure 20 shows the depth profile for F in the intervesicular basalt, a uniform F concentration similar to that of the vesicles' at 1 micron depth, with no indication of a surface peak. Figure 21 gives the results for the vesicle wall and intervesicular rock of sample 15016. Although there is a possibility of a small surface F peak on the intervesicle area, it is much smaller than the surface enhancement on the vesicle wall; overall, the result is quite similar to that of 15556. The interior fluorine concentration of the rock is roughly twice that of the vesicle (Table 4), which can be explained by variations due to the small volume of sample analyzed (5×5×0.001 mm). This variance was also observed for the solid Murchison carbonaceous chondrite results (Chapter III).

The surface F concentrations found on the vesicles are an order of magnitude lower than those observed on green and orange glass spheres. This can reflect a differing composition of the gases responsible in the two cases for forming thin F layers, or, more likely, a difference in condensation efficiencies due to cooling time differences. The fact that the vesicles are surface (< 0.3 μm) enhanced in F indicates that the F-bearing vapor was one of the last to condense in the lunar basalt. This will be further explored in the next chapter.

V. DISCUSSION

The results of fluorine depth probes on lunar samples described in the previous chapter can be discussed in terms of one of three origins: Teflon contamination, fluoride vapor fixation on soil samples, and fluorine fixation on vesicle surfaces. With the possible exception of sample 76215,32 (see Table 3), all of the samples returned from the lunar surface in Teflon bags and packaged by the Lunar Curatorial Facility are apparently contaminated. Two constraints put on samples requested for the study of fluorine on the surfaces of lunar samples were that they be unexposed to F-bearing materials during transport and preparation, and that they be of volcanic origin. When these requirements were met, meaningful results were obtained of fluorine concentrations of Apollo 15 green glass soil, Apollo 17 orange glass soil, and vesicular basalts. Evaluation of these experimental measurements will be made from two standpoints: comparison of the surface films found on the orange and green glasses to other measurements on these samples, and speculation on the formation of lunar basalt vesicles. This topic is not discussed at depth in the lunar science literature, as opposed to the thorough investigation of orange and green soils. Water leaching experiments on these samples were done to attempt to duplicate the results of Jovanovic et al. (1976) and to set constraints on the fluoride chemistry of surface films observed; this work is described below.

Water Leaching Experiments

Although the experimental method employed in this work allows only the measurement of fluorine on sample surfaces, several conclusions can be drawn from water leaching experiments with regard to the chemical composition of the F-rich layers observed. Thermodynamic calculations of the composition of the lunar vapor phase are composition-dependent, and therefore these chemical data would provide a test of theories on lunar magma solidification and vapor condensation. Meyer et al. (1975) and Chou et al. (1975) discuss these surface layers in terms of halide sublimates.

The calculations of Naughton et al. (1972) of mole fractions of major element equilibrium components in a lunar vapor phase provide a list of compounds which, though possibly not completely valid for an Apollo 17 lunar magma, would indicate ratios of halide species. According to the Naughton et al. (1972) table, the most abundant fluoride species would be, respectively: CaF, AlOF, TiOF, FeF, and HF. A series of experiments to compare the water solubility of thin films of these fluorides with the water solubility of the F-rich surface layers on Apollo 15 green glasses and Apollo 17 orange glasses could establish constraints on the halide chemistry of sample surfaces. Jovanovic and Reed (1974) reported that 40% of bulk rock fluorine of a 74220 sample was leachable in a mildly acidic solution (pH 5); subsequent hot water leaching (Jovanovic et al., 1976) was able to remove 20% of the fluorine in a 15427 sample.

Water leaching was performed on > 100 micron fractions of 15427,39 and 74220,235 using high-purity quartz glass distilled water collected by F. Tera of Caltech. Along with each lunar sample leach a quartz disc was exposed to the water and confirmed that the water and apparatus were F-free. First attempts involved 5-minute leaching with room temperature water, and subsequent leaching was done for 10 minutes in hot (80-90°C) water. Fluorine concentration versus depth profiles were measured for both samples after each leach but were essentially unchanged by the process. Owing to the uncertainties of the packing fraction of the glass beads in the beam spot, an upper limit of 20% is placed on the water solubility of the fluorine on these sample surfaces. Since the solubility of CO_2 in water tends to give the solution a slight acidity, the pH 5 leach results of Jovanovic and Reed are surprising. A plausible explanation is that their results are biased to the finer size fractions, which would be etched more by the leaching, and which our experimental method does not sample. Since the results for the > 175 micron size fraction for sample 15427,39 do not point to an inverse grain size dependence of surface F concentration, this is an unlikely cause for the discrepancy. The measurements performed in this study are unambiguous, since they are a straightforward before and after comparison of the same sample. Thus, it can be concluded that these F-rich surface films are water insoluble.

Although the water solubilities of the fluorides mentioned as being prominent in lunar magma are tabulated, the solubility of a thin film deposited on a glass substrate may be different. Since the rate

of solubility is also important in the short time water leaches done on lunar glasses, vapor deposited fluoride films (15-20 $\mu g/cm^2$ each of CaF_2, MgF_2, CrF_2, TiF_3) on glass backings were prepared to measure their response to the water leaching performed on the lunar samples. Counting rates of both cations and fluorine were measured with an electron microprobe for washed and unwashed samples. To duplicate the lunar sample treatment, the films were exposed for 5 minutes in room temperature water, 10 minutes in hot (80-90°C) water, and 30 minutes in hot water (the CaF_2 samples were leached for 5 instead of 10 minutes). All of the films were removed, although the 30-minute hot water leach was required to completely dissolve CaF_2. The CrF_3 and TiF_3 hydrolyzed rather than dissolved, as both Ti and Cr rich particles were observed without the presence of fluorine, possibly in the form of TiO_2 and Cr_2O_3. MgF_2 dissolved completely in the 5-minute room temperature water leach, as expected from its high solubility; presumably other highly soluble fluorides such as ZnF_2 or alkali fluorides would have a similar behavior. Insoluble fluoride species such as FeF_2, AlF_3, AlOF, or $2AlFO \cdot SiO_2$ have not yet been ruled out as candidates for lunar surface films. The alcohol insolubility of the lunar deposits makes AlF_3 an unlikely choice; FeF_2 would be expected to oxidize/hydrolyze on exposure to terrestrial atmosphere.

These experiments are rather simplistic in their approach. It may be that a monolayer of fluoride is able to adhere to the glass substrate, and would be undetected by the relatively insensitive electron microprobe. Taken at face value, these results do not support the idea

of simple halide sublimates discussed by Meyer et al. (1975). The lunar deposits may be altered chemically from those simulated above by the presence of atomic sulfur, which would resist water leaching. Chlorides are readily water soluble, so that fluoro-chloro salt mixtures are unlikely. More exotic chemical forms such as sulfo-fluorides and oxyfluorides cannot be ruled out by this work.

Orange and Green Glass Fluorine Fixations

The substantial fluorine surface films observed on the orange and green glass soils are additional evidence of a volcanic origin. In addition to fluorine the following elements are documented as residing on these samples' surfaces: Zn (Meyer et al., 1975; Chou et al., 1975); Pb (Meyer et al., 1975); K, Cl, ^{36}Ar, ^{40}Ar (Podosek and Huneke, 1973); Cd, In, Ge, Au (Chou et al., 1975); S (Grant et al., 1974; Butler and Meyer, 1976). Although it is important to determine the chemistry/minerology of the surface deposits to better understand the volcanic process, a quantitative chemical assessment is difficult. These samples exhibit heterogeneous distributions of volatile elements and comparison of data measured on different samples is dangerous. A complete chemical analysis is not available and many of the data referred to above are not quantitative surface concentrations. If taken at face value, these data indicate a large excess of anions over cations; a more likely interpretation is that a major element cation (Fe, Ti, or Al) has gone undetected. McKay et al. (1973) reported detection of Fe-rich blobs on 15401 green glass particles but were

unable to determine a chemical form of these blobs, other than the possibility that they were silicates. Also, they failed to confirm previous observations of KCl and Ti-rich particles by Carusi et al. (1972), and their speculation on the presence of metal halide sublimate deposits (Meyer et al., 1975) does not agree with the water leaching experiments described in the previous section.

In an effort to simulate the type of fluorine fixation which would account for the surface fluorine observed, hydrolysis was attempted, since it is a likely candidate for the chemical process needed to attach fluorine to the glassy samples. Naughton et al. (1972) include HF as a component in lunar volcanic vapor, and HF would readily react with the samples. Hydrolyzable fluorides such as TiF_4 or CrF_2, when exposed to the terrestrial atmosphere, could react with water vapor to form HF. Reacting with SiO_2, this would produce SiF_4 which would be lost, implying that a much higher fluorine content could have existed on sample surfaces while on the moon. However, owing to the small concentrations of HF in volcanic vapor relative to the amount of glass present, incomplete reaction could occur forming fluorosilicates, which would be retained.

Silica glass discs were dipped in a dilute (0.5%) HF solution for 1, 10, and 100 seconds to examine the effect of HF on glass, especially with regard to possible fluorine retention. This HF concentration was chosen to yield 10^{14} HF molecules/cm^2 on instantaneous exposure to the solution. After dipping the glass discs were rinsed in water and methanol. The results of this simulation experiment are shown on Figure 22. All the SiF_4 produced would have escaped, and Si-F volatile

compounds would have been pumped away by the 10^{-10} torr vacuum in the target chamber. However, the one-second dip fixed a low amount of fluorine on the glass surface, and the 100-second dip exhibits a surface F layer of 10^{15} atoms/cm^2, comparable to that observed on the orange glasses. The 10-second dip gave results similar to that of the 1-second exposure. Thus, the idea of formation of fluoro-silicates by a hydrolysis mechanism involving terrestrial H_2O and metallic fluorides, or by reaction with HF in lunar volcanic vapor, is qualitatively viable.

Origin of Vesicular Basalts

Whereas the lunar science literature contains a large number of papers on the lunar volcanic glasses and their origins, very little work has been done concerning vesicular basalts and the gases which produce them. The identity of these gases is not obvious, but from observations of size of vesicles and the magnitude and nature of fluorine deposits on their surfaces, several constraints can be placed on their formation (Goldberg et al., 1976).

First, the observations of meter-sized vesicular basalts at the Apollo 15 site (ALGIT, 1972) require that vesicles must have been made at least 1 meter deep in a lava flow. The hydrostatic equilibrium pressure ($p = h\rho g$) at this depth, 0.05 atmospheres, would correspond to gas bubble concentrations of 4.5×10^{-7} moles/cc rock at 1350°K solidus temperature. Second, based on the fact that there is no volume (i.e., > 1 μm depth) enhanced fluorine in vesicle walls or host basalt, the gases must have been in residence longer than the time of crystal formation in the vesicle linings. Since the vesicle and vug wall minerals are highly variable (Schmitt et al., 1970; Skinner, 1970; McKay et al., 1972; Papike et al., 1972), though typical rock forming minerals, a variety of gases must have contributed to vesicle formation, or the gas escaped from the rock. Therefore, the gas must be relatively noncondensable in the rock and on vesicle walls.

Fluorine and fluoride compounds must have been among the last to condense, since enhanced F is found only on vesicle wall surfaces (15016 and 15556 data, Chapter IV). Using the areal concentrations

of Table 4 for thin films found on 15016 and 15556 vesicles (and using a 6 mm average bubble diameter), the gas concentration would be 3×10^{16} atoms per cc, or a factor of ~ 150 less than that required to form such a bubble at 1 meter depth. Thus it would seem that most of the gas forming the vesicle escaped before condensing on the walls. However, the results of water leaching experiments point to a non-volatile F component, which would not have escaped from the vesicle, but would be bound to the silicate material. Therefore, the vesicle forming gases could not consist of F compounds alone, but would likely be present at the 0.6% level (or lower) implied above.

Several other gases can be considered for vesicle formation. Sulfur, although an abundant volatile in vesicular basalts, would have a low partial pressure (10^{-4} atm; see Brett, 1975), and excess sulfur would appear in an Fe-FeS liquid. Thus S can be ruled out as a vesicle-forming gas. Solar wind gases, dominated by H_2, are a possibility. The basalts brought back would represent an accumulation of the last volcanic flow (10 meters deep - Lofgren et al., 1975). Using a time span of 4×10^8 years for lunar volcanism (Tera et al., 1974) over which time 10 km of mare basalt formed, an average time between flows would be 4×10^5 yr. This allows accumulation of 1.3×10^{21} atoms H/cm^2 from the solar wind, or 1×10^{-3} moles H_2/cm^2. This would allow, if averaged over 10 meters thickness, vesiculation at 2 meters depth, well within reason. However, the fact that metallic iron, the result of hydrogen induced chemical reduction, is too abundant (Gibson et al., 1975) relative to steady-state hydrogen concentration (Epstein and

Taylor, 1973), indicates large hydrogen losses. A more general source of vesicular gas is necessary.

Carbon monoxide, the second most abundant gas in lunar volcanic vapor (Naughton et al., 1972) next to S_2, is a possibility. Taking 20 ppm carbon as the lunar basalt concentration, and the fact that most carbon is released during acid hydrolysis experiments as CO and CO_2, CO could be present at the 5×10^{-6} moles/cc level. This would form bubbles at 10 meters depth (see above). However, the Gibson et al. data show no correlation between vesicularity and carbon content, indicating large gas losses. Other gaseous species such as N_2 or Ar are possibilities, but a more general mixture is indicated by the various conditions present on the moon.

VI. CONCLUSIONS

The high surface fluorine concentrations that have been observed on the Apollo 15 green glass samples and the Apollo 17 orange glass samples are most easily understood in terms of a volcanic origin. The hypothesis of Heiken et al. (1974) and Meyer et al. (1975) of a lava fountain mechanism produced by a partially melted liquid inside the moon is a plausible explanation for fixing fluoride compounds on the glass particle surfaces. The overall arguments for a volcanic origin are (McKay et al., 1973):

(1) The green glasses are enriched in volatile elements, among them fluorine, found in large abundance in this study. The green glasses are relatively poor in C, N, H, and rare gases (Wszolek et al., 1972; Lakatos and Heymann, 1972; DesMarais et al., 1975). This shows that the green and orange soils have not had a long history of exposure to the solar wind. In addition, the major component of the soils is homogeneous glass spheres, which argues for a unique and common origin for the spheres and the volatiles they contain. The overall high volatile concentrations qualitatively match those expected for lunar volcanic vapor (Naughton et al., 1972). This is quite different from an impact generated outgassing event or heterogeneous input from meteorite impact.

(2) The age of the 15426 green glass corresponds to the period of volcanic activity at the Apollo 15 site (Podosek and Huneke, 1973).

(3) The green and orange glasses' composition is very rare at the lunar surface (Green and Ringwood, 1973); i.e., there is no source

rock on the moon's surface from which the glasses could be produced by impact.

The arguments for a volcanic origin of the green and orange glasses, and the large fluorine surface films found on them make it quite plausible that the fluorine observed on the Surveyor VII experiments (Patterson et al., 1970) was real and of lunar volcanic origin. Since the large majority of samples examined in this work were contaminated, the interpretation that the Surveyor VII lunar highlands measurements were fluorine contaminated by spacecraft outgassing must be considered.

The magnitude of F surface films on vesicular basalt surfaces point to a number of different conclusions examined in the previous chapter. Different source gases, cooling rates and condensation efficiencies can be argued for the basalts and green and orange glasses. The experimental evidence correlating F surface films with these samples supports the idea of volcanic origin for them, but the subject of the chemistry involved in fixing the F atoms to sample surfaces is open to discussion.

The inconclusive results obtained in measuring carbon on the surfaces of lunar and terrestrial materials nevertheless show that previous measurements of carbon by other techniques may be compromised by terrestrial gas absorption. A method of effectively pumping away and trapping carbon-rich gases from sample surfaces must be developed before a direct measurement of solar wind carbon implanted in lunar samples can be accomplished. The sample handling methods of the lunar

science program make consideration of contamination an ever-present necessity.

APPENDIX I

The following is a brief discourse on the derivation of a resonant yield in a nuclear reaction, as, for example, in Brewers and Flack (1969).

With a resonance of a Breit-Wigner shape,

$$\sigma(E) = \sigma_R \frac{\Gamma^2/4}{(E - E_R)^2 + \Gamma^2/4} , \qquad \text{(AI:1)}$$

where the cross section $\sigma(E)$ refers to an isolated resonance of peak cross section σ_R, width Γ, at energy E_R. The yield from a reaction such as $^{19}F(p,\alpha\gamma)^{16}O$ is given by

$$Y = \int_{E^-}^{E} \frac{\sigma}{\varepsilon} \, dE \qquad \text{(AI:2)}$$

with $\varepsilon = \frac{1}{N} \frac{dE}{dx}$, the stopping cross section of the target, and N is the number of target nuclei. If this stopping cross section does not vary with energy over the resonance,

$$Y = \int_{E^-}^{E} \frac{\sigma(E)}{\varepsilon} \, dE = \frac{1}{\varepsilon} \int_{E^-}^{E} \sigma_R \frac{\Gamma^2/4}{(E - E_R)^2 + \Gamma^2/4} \, dE$$

$$= \frac{\sigma_R}{\varepsilon} \frac{\Gamma^2}{4} \int_{E-\xi}^{E} \frac{dE}{(E - E_R)^2 + \Gamma^2/4} .$$

Integrating over E,

$$Y = \frac{\sigma_R \Gamma}{2\varepsilon} \left[\tan^{-1} \frac{(E - E_R)}{\Gamma/2} - \tan^{-1} \frac{(E - E_R - \xi)}{\Gamma/2} \right] . \qquad \text{(AI:3)}$$

If $\xi >> \Gamma$ (i.e., if the energy difference integrated over is much larger than the width of the resonance):

$$Y_{max} = \frac{\pi}{2} \frac{\sigma_R \Gamma}{\varepsilon} = \frac{\pi}{2} \frac{\sigma_R \Gamma}{dE/dx} N \quad . \qquad (AI:4)$$

Thus the gamma ray yield is directly proportional to the atomic concentration. The number of gamma ray counts observed N_γ equals:

$$N_\gamma = f \mu \eta Y n \quad , \qquad (AI:5)$$

where n = number of incident protons.

μ = correction for γ-ray absorption, other γ-ray yielding reactions which are non-isotropic.

f = fraction of all γ-ray detector counts falling in selected integration window.

η = fraction of γ-rays emitted by target which interact with the detector.

The resonance parameters given by Chao et al. (1950) give a total yield of 37×10^{-8} gamma rays per incident proton for the $^{19}F(p,\alpha\gamma)^{16}O$ 872 keV resonance.

Thus, the thick target yield of 2.55×10^5 counts for 2 microcoulomb integrated proton bombardment implies a "detection efficiency" $\eta' = f \mu\eta$ of 0.055 for the experimental configuration employed.

If a second resonance is found at a higher energy E_{R_2}, then the total yield $Y(E) = Y_1(E) + Y_2(E)$. Since the resonances will react with target nuclei at different depths,

$$Y_1(E) = \frac{\pi}{2} \frac{\sigma_{R_1} \Gamma_1}{(-dE/dx)_1} N(x_1) \quad , \tag{AI:6}$$

$$Y_2(E) = \frac{\pi}{2} \frac{\sigma_{R_2} \Gamma_2}{(-dE/dx)_2} N(x_2) \quad , \tag{AI:7}$$

where the different subscripts refer to parameters of the different resonances, and

$$x_1 = \int_{E_{R_1}}^{E} \frac{dE}{(dE/dx)_1} \quad , \tag{AI:8}$$

$$x_2 = \int_{E_{R_2}}^{E} \frac{dE}{(dE/dx)_2} \quad , \tag{AI:9}$$

so that

$$x_2 = x_1 - \int_{E_2}^{E_1} \frac{dE}{(dE/dx)} = x_1 - \Delta x \quad . \tag{AI:10}$$

Therefore,

$$Y_2 = \frac{\pi}{2} \frac{\sigma_{R_2} \Gamma_2}{(dE/dx)_2} N(x_1 - \Delta x)$$

and this can be subtracted from the total yield to obtain the yield due to resonance 1 alone, extending the probe of resonance 1 to greater depths.

The energy loss values are calculated from the tabulation by Northcliffe and Schilling (1970). Values for nuclei of intermediate z are obtained by linear interpolation, and for a material of complex

composition such as a lunar or meteoritic sample,

$$\frac{dE}{d(\rho x)}_{sample} = \sum_i f_i \left(\frac{dE}{d\rho x}\right)_i \quad .$$

Here, $dE/d(\rho x)$ refers to an energy loss as given by the Northcliffe and Schilling table, f_i is the weight fraction of element i with stopping power $(dE/d(\rho x))_i$.

APPENDIX II

For the purpose of calibrating detection efficiencies and converting count rates to concentrations, several standard targets have been used:

1. Reagent CaF_2 - 300 $\mu g/cm^2$ deposited by vacuum evaporation on a tantalum substrate; 15 $\mu g/cm^2$ deposited by vacuum evaporation on a quartz substrate.
2. Durango apatite - 5/8" diameter chip (54.02% CaO, 40.78% P_2O_5, 3.53% F, 1.43% RE_2O_3, plus minor elements < 1% total - Leich, 1974).
3. Thin film carbon - 11.2 $\mu g/cm^2$ carbon foil on a quartz glass substrate.
4. Hilton deposit calcite - 1/2" diameter chip of $CaCO_3$, stoichiometrically 12.00% carbon by weight.

The above targets have been used in converting counts to atoms F/cm^2, ppmF, atoms C/cm^2, and ppm C, and in calculating the detection efficiency of the NaI(Tl) detector used in $^{19}F(p, \alpha\gamma)$ study, as described in Appendix I.

APPENDIX III

Whereas in the technique using the reaction $^{19}F(p,\alpha\gamma)$ only the proton energy loss and straggling need be considered in evaluating depth and resolution, in the backscatter experimental technique utilizing $^{12}C(d,p_0)$, several factors are considered. First is the relationship between E_d, the deuteron bombardment energy, and E_p, the reaction product proton energy backscattered at 160° lab angle. Using the appropriate equations from Marion and Young (1968) for relativistic kinematics of two-body reactions, in the region of interest (E_d = 0.8 - 1.5 keV), $dE_p/dE_d = 0.588$. Thus at the reaction site within the sample, $E_p = E_{p_{max}} + 0.588\ (E_d - E_{d_0})$, where $E_{p_{max}}$ is the reaction product proton energy at the sample surface with bombarding deuteron energy E_{d_0}, and E_d is the deuteron energy at the reaction site. The depth Δx at which the reaction takes place is given by

$$\Delta x = \frac{E_d - E_{d_0}}{(dE/dx)_d} \qquad \text{(AIII,1)}$$

where $(dE/dx)_d$ is the energy loss of the deuteron beam in the sample (a negative quantity). The path length of the protons scattered at 160° in exiting the sample is simply $\Delta x/\cos 20°$, so that the loss of energy of the protons is $\Delta x \sec 20''\ (dE/dx)_{p.s.}$, where $(dE/dx)_{p.s.}$ is the rate of proton energy loss in the sample.

$$E_p = E_{p_{max}} + 0.6(E_d - E_{d_0}) + \Delta x \sec 20°\ (dE/dx)_{p.s.} \qquad \text{(AIII,2)}$$

as the protons enter the entrance foil to the detector. The additional loss in the foil, used to stop backscattered elastic deuterons, is given by $(dE/dx)_{pf} \times t_f$ (dE/dx_{pf} = energy loss rate of protons in the foil; t_f = foil thickness). Finally, the proton energy as seen by the detector is

$$E_p = E_{p_{max}} + 0.6(E_d - E_{d_0}) + \Delta x \sec 20° \, (dE/dx)_{p.s.} + (dE/dx)_{p.f.} \, t_f \qquad \text{(AIII,3)}$$

The width of the proton group from the reaction $^{12}C(d,p_0)$ would be a sum in quadrature of detector resolution, deuteron straggling, and proton straggling, both in the sample and in the foil.

APPENDIX IV

The problems of maintaining target cleanliness (avoiding contaminants) and an ultra-high vacuum, as well as containing the various types of lunar samples require special experimental apparatus and techniques. As mentioned in Chapter II, all materials used in the target chamber are vacuum bakeable to 300°C; bakeout is performed periodically to remove surface adsorbed gases. The components are cleaned in various appropriate solvents: trichloroethylene for degreasing, acid etching on metallic surfaces, and high-purity methanol as a final cleaner. Methanol is used to clean all tools employed in target manipulation, as well as some samples (as mentioned in Chapters IV and V) which are water rinsed or ultrasonically rinsed to remove adhering dust particles. During all phases of vacuum system and target handling polyethylene gloves were worn to keep fingerprints from the pristine surfaces. In addition, whenever the vacuum system was opened to load targets, it was vented and flushed with a 5 psi flow of dry nitrogen after passing through a copper tube coil immersed in liquid nitrogen. This procedure traps water vapor and CO_2, but does not remove any possible CO, which would be necessary in the carbon depth probe work (Chapter II).

When sample containers were received from the Lunar Curatorial Facility, in general they were opened in the dry nitrogen glove box in S. Epstein's laboratory at Caltech. In cases where atmospheric exposure was to be strictly avoided, the samples were mounted in their target holders inside the glove box, transported to the tandem

accelerator laboratory in closed polyethylene bags, and placed in the target chamber with an attached glove bag which was flushed with nitrogen for several minutes prior to opening the poly bags.

While most of the samples studied in this work were several millimeters in size and easily handled by standard procedures mentioned in Chapter II, the 15427 and 74220 100 micron size soil samples presented new problems. Handpicking green and orange glass separates was done under a binocular microscope in a "clean" room with methanol washed tools. Samples were mounted behind stainless steel mesh, with either 175 μm or 100 μm size openings, which were used to size separate the soil particle samples. The first method employed in mounting these samples for proton beam bombardment was to drop the glass beads into a quartz glass collimated hole with screen at the bottom, and restrain the beads with aluminum foil, so that the beam would pass through the screen and subsequently hit the sample. Precise positioning of the beam spot was enabled by avoiding the fluorescing quartz collimator. A second, improved method contained the 100 micron size particles in a 200 micron deep, 3 mm diameter recess in a stainless steel flat-bottomed cup. The screens were placed over the recess, a quartz collimator (with hole size equal to the recess diameter) over the screen, and a beryllium-copper spring clip restrained this "sandwich". It was found that this holder arrangement restrained the soil particles very effectively during sample holder transport and proton bombardment.

The beam transmission of the screens was measured by CaF_2 thick target yields in screened and unscreened conditions. (Correction

factors of 3.07 for the 100 micron size and 2.96 for the 175 micron size screens are applied when necessary.)

APPENDIX V

When measuring the count rate for a standard target (CaF_2 or apatite) using the reaction $^{19}F(p,\alpha\gamma)^{16}O$, 100% of the proton beam measured by the current integrator is incident on the sample. While this is also true for most of the lunar and meteoritic samples probed in this experimental work, such is not necessarily the case for the Apollo 15 green and the Apollo 17 orange soil samples. While the beam transmission of the screens used to hold the samples is known (Appendix IV), the packing efficiency of the glass particles behind the screen is not known. Visual estimates can be made under binocular microscope examination, but this is done while the sample orientation is horizontal rather than vertical, the position assumed in the target chamber.

A direct measurement of the packing efficiency can be made using the reaction $^{16}O(d,p)$, and detecting backscattered protons with the silicon surface-barrier detector mounted in the vacuum system for carbon analysis. The $^{16}O(d,p)$ reaction, with a Q-value of 1.918 MeV, has two particle groups at the 1.07 MeV deuteron bombardment energy (see Figure 23). These are well separated from the $^{12}C(d,p_0)$ group, and by relating the proton yield from a screen covered quartz glass disc to that of the orange or green glass samples (taking relative oxygen abundances into account), the fraction of a glass sample bombarded by the typical beam spot is measured. Corrections of 0-67% for fluorine concentrations have been applied to those samples assayed in this manner (74220,174; 74220,235 brown fragments; 15427,39 brown glass).

APPENDIX VI

A number of reactions were studied for the purpose of experimentally probing lunar samples for carbon. For various reasons, all of the below reactions were rejected for use in carbon analysis before the $^{12}C(d,p_0)^{13}C$ probe was perfected (see Table 1).

1. $^{12}C(^{3}He,n)^{14}O \xrightarrow[\beta+]{} {}^{14}N^{*} \xrightarrow{\gamma} {}^{14}N_{g.s.}$ This reaction utilized a ^{3}He beam to produce the ^{14}O nucleus, which decays with a half-life of 71 seconds via positron emission to the first excited state of ^{14}N. The delayed gamma rays are counted in two successive half-life intervals after a pause to allow any short half-life nuclei produced to decay and the successive half-life count rates are subtracted to eliminate long-lived decays. The yield below a 2.3 MeV resonance (^{3}He lab energy) is subtracted from the above resonance yield to obtain a carbon sensitivity. The problems encountered in this reaction are long counting times, energy dependent background, low sensitivity, and activation of the NaI(Tl) detector due to neutron irradiation, producing a competing gamma ray from ^{23}Na neutron capture within the crystal. This produced a long-lived (15-hour) background of 2.75 MeV gamma rays which increased with irradiation times.

2. $^{12}C(^{3}He,p\gamma)^{14}N$ - This reaction populates excited states of ^{14}N using a ^{3}He beam, which again causes NaI(Tl) crystal activation described above. A resonance of 3.0 MeV producing 6.44 MeV gamma rays, with a 130 keV width, was examined. A large, exponential rise in the gamma ray yield from other reactions was observed as beam energy was increased from below to above the resonance, making subtraction of the

$^{12}C(^{3}He,p\gamma)$ yield difficult.

3. $^{12}C(d,p\gamma)^{13}C$ - This reaction produces 3.1 MeV gamma rays from the first excited state of ^{13}C. Not only was the background radiation strongly energy dependent, but composition dependent as well, making background subtraction over the step in the $^{12}C(d,p\gamma)$ yield very difficult.

4. $^{13}C(^{3}He,\alpha)$ - This reaction was a first attempt to use reaction producing particles rather than gamma rays. Backscattered alphas were detected with a silicon surface barrier detector. Although there were not other competing alpha-producing reactions, large proton fluxes were observed, which caused a large number of pile-up pulses in the detector. The high center-of-mass energy of the reaction would necessitate very low beam currents to limit sample heating. Finally, the reaction measures ^{13}C, which is a 1% abundant isotope of carbon, which coupled with the reaction's low yield meant the sensitivity was far too low to detect the surface C layers found in lunar samples.

REFERENCES

Ajzenberg-Selove, F. 1971, Nucl. Phys. A166, 1.

ALGIT (Apollo Lunar Geology Investigation Team) 1972, The Apollo 15 Preliminary Science Report, NASA SP-289.

Amsel, G., Béranger, G., de Gélas, B, and Lacombe, F. 1968, J. Appl. Phys. 39, 2246.

Anders, E. 1964, Space Sci. Rev. 3, 583.

Beckner, E. H., Bramblett, R. L., Phillips, G. C., and Eastwood, T. A. 1961, Phys. Rev. 123, 2100.

Bibring, J. P., Borg, J., Burlingame, A. L., Langevin, Y., Maurette, M.,and Vassent, B. 1975, Proc. 6th Lunar Sci. Conf., 3471.

Brett, R. 1975, Lunar Science VI, 89.

Brewers, J. M., and Flack, F. C. 1969, The Analyst 94, 1.

Butler, P. 1975, private communication.

Butler, P. and Meyer, C. 1976, Lunar Science VII, 114.

Carusi, A., Cavaretta, G., Cinotti, F., Civitelli, G., Coradini, A., Fulchignoni, M., Funiciello, R., Taddeucci, A., and Trigila, R. 1972, The Apollo 15 Lunar Samples, 5.

Cavarretta, G., Funiciello, R., Giles, H., Nicholls, G. D., Taddeucci, A., and Zussman, J. 1972, The Apollo 15 Lunar Samples, 202.

Chao, C. Y., Tollestrup, A. V., Fowler, W. A., and Lauritsen, C. C. 1950, Phys. Rev. 79, 108.

Chou, C. L., Boynton, W. V., Sundberg, L. L., and Wasson, J. T. 1975, Proc. 6th Lunar Sci. Conf., 1701.

DesMarais, D. J., Hayes, J. M., and Meinschein, W. G. 1973, Proc. 4th Lunar Sci. Conf., 1543.

DesMarais, D. J., Basu, A., Hayes, J. M., and Meinschein, W. G. 1975, Proc. 6th Lunar Sci. Conf., 2353.

Eberhardt, P., Geiss, J., Graf, H., Grögler, N., Krähenbühl, U., Schwaller, H., Schwarzmüller, J., and Stettler, A. 1970, Proc. Apollo 11 Lunar Sci. Conf., 1037.

Epstein, S. and Taylor, H. P. 1973, Proc. 4th Lunar Sci. Conf., 1559.

Epstein, S. and Taylor, H. P. 1975, Proc. 6th Lunar Sci. Conf., 1771.

Fisher, D. E. 1963, J. Geophys. Res. 68, 6331.

Gibson, E. K., Chang, S., Lennon, K., Moore, G. W., and Pearce, G. W. 1975, Proc. 6th Lunar Sci. Conf., 1287.

Goldberg, R. H., Burnett, D. S., Tombrello, T. A., and Furst, M. 1974, Meteoritics 9, 347.

Goldberg, R. H., Burnett, D. S., and Tombrello, T. A. 1975, Proc. 6th Lunar Sci. Conf., 2189.

Goldberg, R. H., Burnett, D. S., and Tombrello, T. A. 1976, Proc. 7th. Lunar Sci. Conf., submitted for publication.

Grant, R. W., Housely, R. M., Szalkowski, F. J., and Marcus, H. L. 1974, Proc. 5th Lunar Sci. Conf., 2423.

Green, D. H. and Ringwood, A. E. 1973, Earth Planet. Sci. Lett. 19, 1.

Greenland, L. and Lovering, J. F. 1965, Geochim. Cosmochim. Acta 29, 821.

Heiken, G. H., McKay, D. S., and Brown, R. W. 1974, Geochim. Cosmochim. Acta 38, 1703.

Jovanovic, S. and Reed, G. W., Jr. 1974, Proc. 5th Lunar Sci. Conf., 1685.

Jovanovic, S., Jensen, K., and Reed, G. W., Jr. 1976, Lunar Science VII, 437.

Kashy, E., Perry, R. R., and Risser, J. R. 1960, Phys. Rev. 117, 1289.

Lakatos, S. and Heymann, D. 1972, The Apollo 15 Lunar Samples, 284.

Larimer, J. W. and Anders, E. 1967, Geochim. Cosmochim. Acta 31, 1239.

Leich, D. A. 1974, Ph.D. Thesis, Caltech (unpublished).

Leich, D. A. and Tombrello, T. A. 1973, Nucl. Inst. and Meth. 108, 67.

Leich, D. A., Goldberg, R. H., Burnett, D. S., and Tombrello, T. A. 1974, Proc. 5th Lunar Sci. Conf., 1869.

Lofgren, G. E., Donaldson, C. H., and Usselman, T. M. 1975, Proc. 6th Lunar Sci. Conf., 79.

Marion, J. B. 1966, Rev. Mod. Phys. 38, 660.

Marion, J. B. and Young, F. C. 1968, Nuclear Reaction Analysis. North Holland Publishing Co., Amsterdam.

McKay, D. S., Clanton, U. S., Morrison, D. A., and Ladle, G. H. 1972, Proc. 3rd Lunar Sci. Conf., 739.

McKay, D. S., Clanton, U. S., and Ladle, G. 1973, Proc. 4th Lunar Sci. Conf., 225.

Meyer, C., Jr., and McKay, D. S. 1974, Meteoritics 9, 382.

Meyer, C., Jr., McKay, D. S., Anderson, D. H., and Butler, P., Jr. 1975, Proc. 6th Lunar Sci. Conf., 1673.

Möller, E. and Starfelt, N. 1967, Nucl. Inst. and Meth. 50, 225.

Naughton, J. J., Hammond, D. A., Margolis, S. V., and Muenow, D. W. 1972, Proc. 3rd Lunar Sci. Conf., 2015.

Northcliffe, L. C. and Schilling, R. F. 1970, Nucl. Data Tables A7, 233.

Ollerhead, R. W., Almqvist, E., and Keuhner, J. A. 1966, J. Appl. Phys. 37, 2440.

Padawer, G. M. 1970, Nucl. Appl. and Tech. 9, 856.

Papike, J. J., Bence, A. E., and Ward, M. A. 1972, The Apollo 15 Lunar Samples, 144.

Patterson, J. H., Turkevich, A. L., Franzgrote, E. J., Economou, T. E., and Sowinski, K. P. 1970, Science 168, 825.

Phillips, W. R. and Read, F. H. 1963, Proc. Phys. Soc. 81, 1.

Podosek, F. A. and Huneke, J. C. 1973, Earth Planet Sci. Lett. 19, 413.

Reed, G. W., Jr. 1964, Geochim. Cosmochim. Acta 28, 1729.

Reed, G. W., Jr. 1975, private communication.

Reed, G. W., Jr. and Jovanovic, S. 1973, Geochim. Cosmochim. Acta 37, 1457.

Schmitt, H. H., Lofgren, G., Swann, G. A., and Simmons, G. 1970, Proc. Apollo 11 Lunar Sci. Conf., 1.

Simoneit, B. R., Neil, J. M., Wszolek, P. C., and Burlingame, A. L. 1976, Lunar Science VII, 815.

Skinner, B. J. 1970, Proc. Apollo 11 Lunar Sci. Conf., 891.

Stauber, M. C., Padawer, G. M., Brandt, W., D'Agostino, M. D., Kamykowski, E., and Young, D. A. 1973, Proc. 4th Lunar Sci. Conf., 2189.

Suess, H. and Urey, H. C. 1956, Rev. Mod. Phys. 28, 53.

Teegarden, B. J., von Rosenvinge, T. T., and McDonald, F. B. 1973, Ap. J. 180, 571.

Tera, F. and Wasserburg, G. J. 1976, Lunar Science VII, 858.

Tera, F., Papanastassiou, D. A., and Wasserburg, G. J. 1974, Earth Planet. Sci. Lett. 22, 1.

Withbroe, G. L. 1971, in Menzel Symposium on Solar Physics, Atomic Spectra, and Gaseous Nebulae, National Bureau of Standards Special Pub. No. 353, 127.

Wszolek, P. C., Jackson, R. F., and Burlingame, A. L. 1972, The Apollo 15 Lunar Samples, 324.

TABLE 1

List of carbon reactions utilized in depth probes of carbon in lunar samples. Parameters indicated are beam energy (center of mass), particle or radiation detected, depth resolution and depth limit of the reaction, and counting sensitivity per microcoulomb per % carbon in the sample. (See text, page 67.)

TABLE 1

Reaction	C.M. Energy (MeV)		Depth Resolution (μm)	Depth Limit	Sensitivity (counts/μC/%C)
$^{12}C(^{3}He,n)$	1.87	2.31 MeV γ's from $^{14}O \xrightarrow{\beta^+} {}^{14}N^*$	0.65	~2	80
$^{12}C(^{3}He,p\gamma)$	2.4	6.44 MeV γ's from $^{14}N^*$	0.33	2.5	1400
$^{12}C(d,p\gamma)$	0.79	3.1 MeV γ's from $^{13}C^*$	0.6	2.3	1300
$^{12}C(d,p_0)$	0.92	3 MeV protons	0.5	2.5	230*†
$^{13}C(^{3}He,\alpha)$	5.4	12 MeV alphas	0.1	~5	0.1

*integrated counts over plateau in $CaCO_3$ proton spectrum

†1.66 counts/μC/10^{15} atoms surface C

TABLE 2

Fluorine concentration data for carbonaceous chondrite meteorites. Since no samples exhibited surface peaks, concentrations quoted are taken from net average yields over the resonance. Typical analytic precision is ± 8%. Carbonaceous chondrite type is also indicated. (See text, page 19.)

TABLE 2

Solid Samples			Crushed Samples		
	F concentration			F concentration	
Sample	ppmF	atoms F/10^6 atoms Si	Sample	ppmF	atoms F/10^6 atoms Si
Murchison*	80	910	Murchison 5*	75	853
Murchison 7b*	72	819	Murchison 6*	60	682
Murchison 7c*	73	830	Murchison 10*	66	751
Murhcison 7d*	80	910	Murchison 11*	59	671
Murchison 7e*	53	603	Mighei*	66	751
Murchison 7f*	93	1058	Essebi*	80	910
Allendé Z1-14†	165	1562	Haripura*	59	671
Allendé Z1-15†	94	890	Ivuna&	70	981
			Orgueil&	74	1037
Murchison average	75.2	855	Allendé†	59	559
Allendé average	129.5	1226			
			Murchison average	65	739
			Type II average	67	762
			Type I average	72	1009
			All crushed average	67	787

&: carbonaceous chondrite Type I

*: carbonaceous chondrite Type II

†: carbonaceous chondrite Type III

TABLE 3

Fluorine concentration data for lunar samples contaminated by Teflon packaging. Exceptions include 66044,8 interior and 70019,17 interior, freshly exposed at Caltech. The two columns of data demonstrate the surface F contamination. (See text, page 22.)

TABLE 3

Sample	Surface Averaged F Content (ppm) 0-0.5 μm	0.5-1.0 μm
65315,6	1000	480
65315,6 interior	100	50
*68124,3-A	410	50
*68124,3-B	850	120
*68124,10-A	260	130
*68124,10-B	220	100
*66044,8-A	820	540
*66044,8-B	1900	1400
*66044,8 interior	75	40
†70019,17	235	60
†70019,17 interior	180	130
†75075,2	975	550
†75075,18	330	150
76215,19	2520	840
76215,32	60	15
76215,33	175	50

*Sealed rock box sample

†Sealed rock box sample; not Teflon bagged

TABLE 4

Fluorine concentration data for uncontaminated lunar samples displaying thin F films. The surface F was obtained by integrating the measured depth profile over the surface peak observed; the volume concentration is an average net yield of data points obtained at greater depths. 1σ errors are indicated. All 15427 and 74220 samples except that indicated were ultrasonically rinsed in high-purity methanol. (See text, page 32.)

TABLE 4

Sample Number	Description	Surface F (10^{15} atoms/cm^2)	Volume F (0.5-1.2 μm) (ppm)
15427,39*	> 175 μm clear green spheres (unwashed)	1.90 ± 0.90	100 ± 30
15427,39*	> 175 μm clear green spheres (washed)	2.80 ± 0.10	33 ± 10
15427,39*	> 175 μm devitrified green glass	6.00 ± 0.15	32 ± 10
15427,39†	> 100 μm clear green spheres	0.76 ± 0.05	72 ± 20
		1.35 ± 0.07	74 ± 20
15427,39&	> 175 μm brown glass	---	67 ± 20
74220,28†	> 100 μm orange glass	0.92 ± 0.06	80 ± 25
74220,235†	> 100 μm orange glass	0.94 ± 0.06	109 ± 35
74220,235&	> 100 μm non-orange glass	---	95 ± 30
74220,174&	> 100 μm unbroken orange spheres	1.35 ± 0.07	52 ± 18
74220,174&	> 100 μm broken orange spheres	0.36 ± 0.04	30 ± 10

*uncorrected for packing, sample holder partially full

†uncorrected for packing, sample holder full

&corrected for packing

(Table continued)

TABLE 4 (continued)

Sample Number	Description	Surface F (10^{15} atoms/cm^2)	Volume F (0.5-1.2 μm) (ppm)
15012,63	brown glass surface	- ±	109 ± 8
15012,63	breccia surface	0.70 ± 0.03	247 ± 10
15012,67	brown glass surface	- ±	73 ± 8
15012,67	breccia surface	0.99 ± 0.04	470 ± 10
15016,176	vesicle	0.10 ± 0.02	44 ± 6
15016,176	intervesicular area	< 0.06	102 ± 7
15556,94	vesicle 1	0.17 ± 0.02	37 ± 6
15556,94	vesicle 2	0.18 ± 0.02	69 ± 6
15556,94	intervesicular area	< 0.05	60 ± 6

FIGURE 1

Depth resolution of the $^{19}F(p,\alpha\gamma)^{16}O$ nuclear reaction analysis technique as a function of depth. Density and energy loss used to calculate this relation are for an average lunar sample composition. The depth resolution calculation includes uncertainties due to proton beam energy spread, width of the resonance, and energy straggling of the beam. (See text, page 6.)

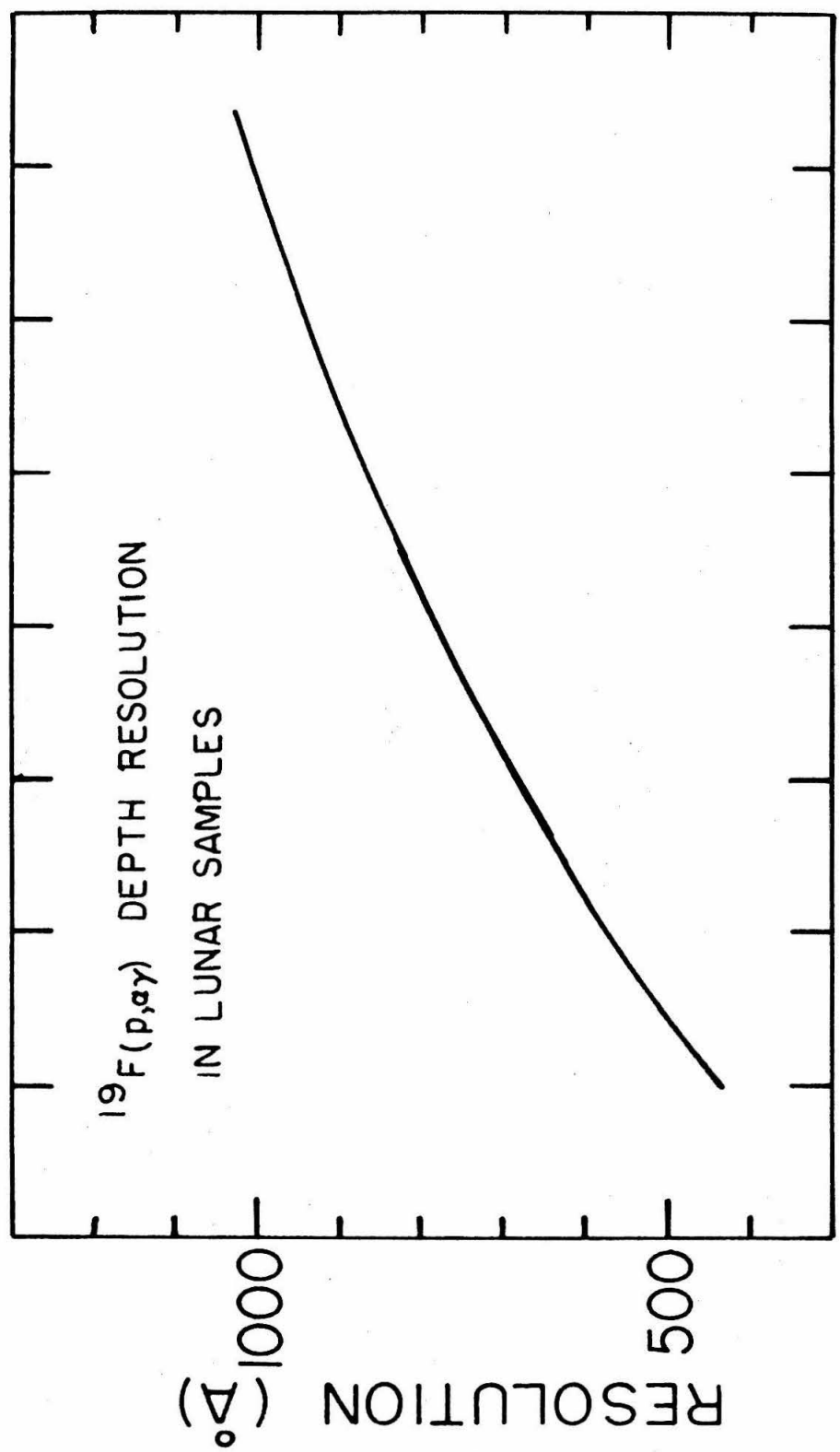
$^{19}F(p,\alpha\gamma)$ DEPTH RESOLUTION
IN LUNAR SAMPLES
RESOLUTION (Å)
1000
500
0
0.4
0.8
1.2
DEPTH (μm)

Figure 1

FIGURE 2

Excitation function for the reaction $^{12}C(d,p_0)^{13}C$ at θ_{lab} = 160°. Data points are taken from integrals of thin carbon target (11.2 μg/cm^2) yields for 20 microcoulombs integrated deuteron beam. (See text, page 9.)

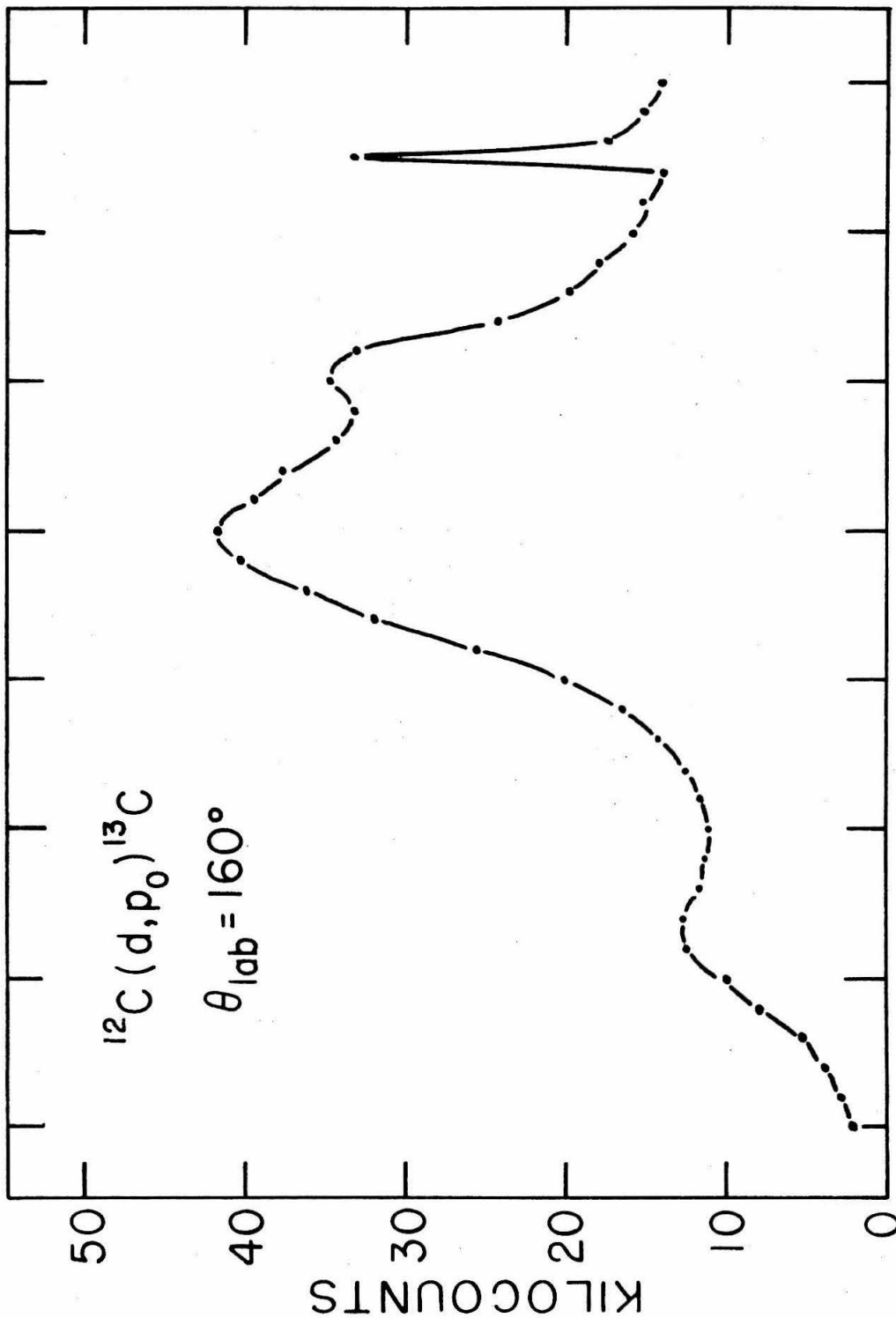
$^{12}C(d,p_0)^{13}C$
$\theta_{lab} = 160°$
KILOCOUNTS
0
10
20
30
40
50
0.8
1.0
1.2
1.4
E_d (MeV)

Figure 2

FIGURE 3

Thin carbon target (11.2 $\mu g/cm^2$) yield curves for the reaction $^{12}C(d,p_0)^{13}C$. Shown are pulse-height spectra taken at deuteron energies of 0.9, 1.07, 1.1, 1.3, and 1.5 MeV. Protons are detected at θ_{lab} = 160° by a 500 micron thick silicon surface barrier detector. All spectra shown are for 20 microcoulombs integrated deuteron beam. Note difference in vertical scales. Spectral widths are due to detector resolution and proton straggling in the entrance foil. (See text, page 9.)

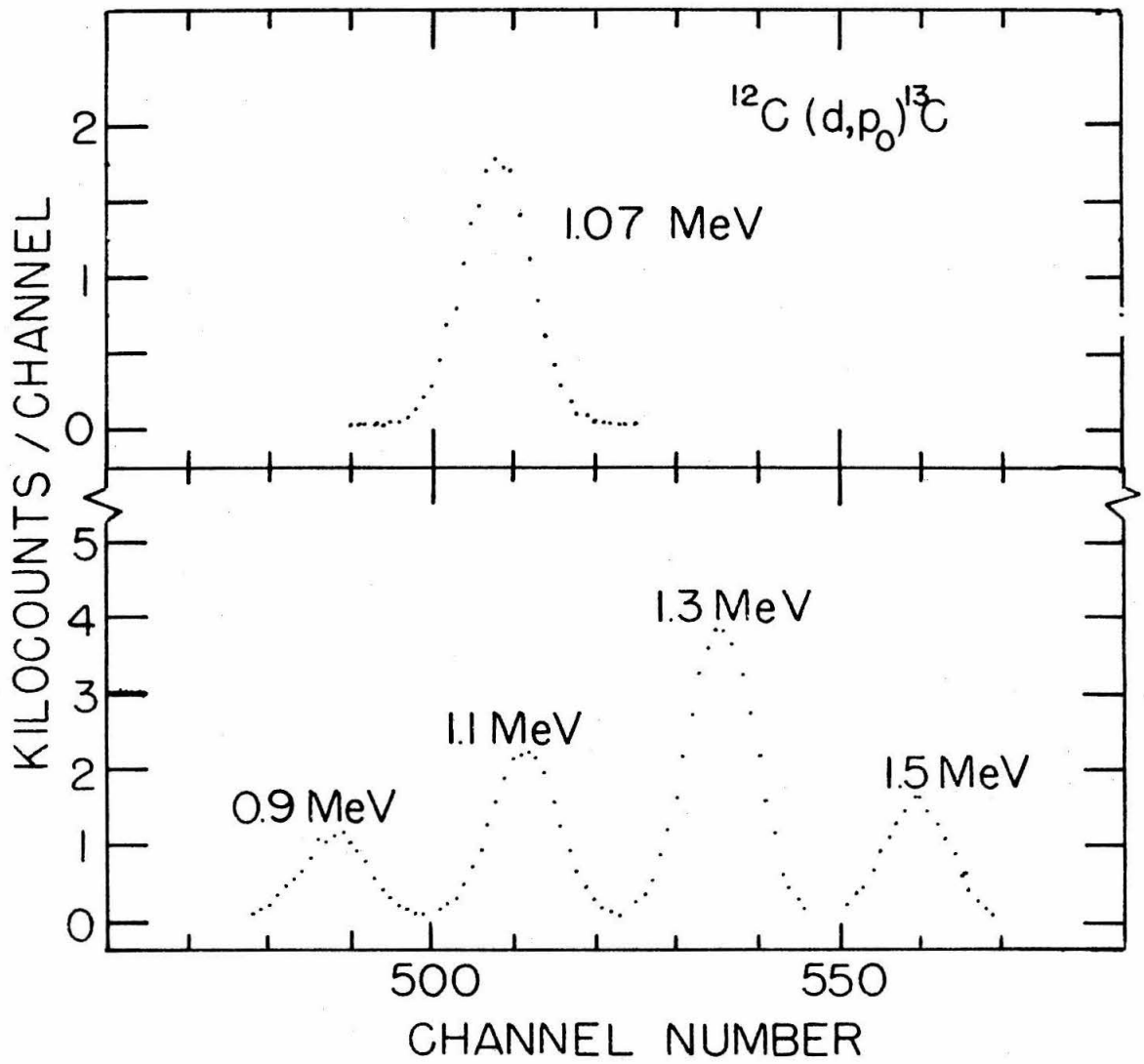
$^{12}C(d,p_0)^{13}C$
1.07 MeV
1.3 MeV
1.1 MeV
1.5 MeV
0.9 MeV
KILOCOUNTS / CHANNEL
CHANNEL NUMBER
500
550
0
1
2
3
4
5

Figure 3

FIGURE 4

Thick carbon target (natural $CaCO_3$) yield curves for the reaction $^{12}C(d,p_0)^{13}C$. Shown are pulse-height spectra taken at deuteron energies of 1.07, 1.2, and 1.5 MeV. Protons are detected at $\theta_{lab} = 160°$ over integrated deuteron charge of 20 microcoulombs. Note difference in vertical scales. (See text, page 9.)

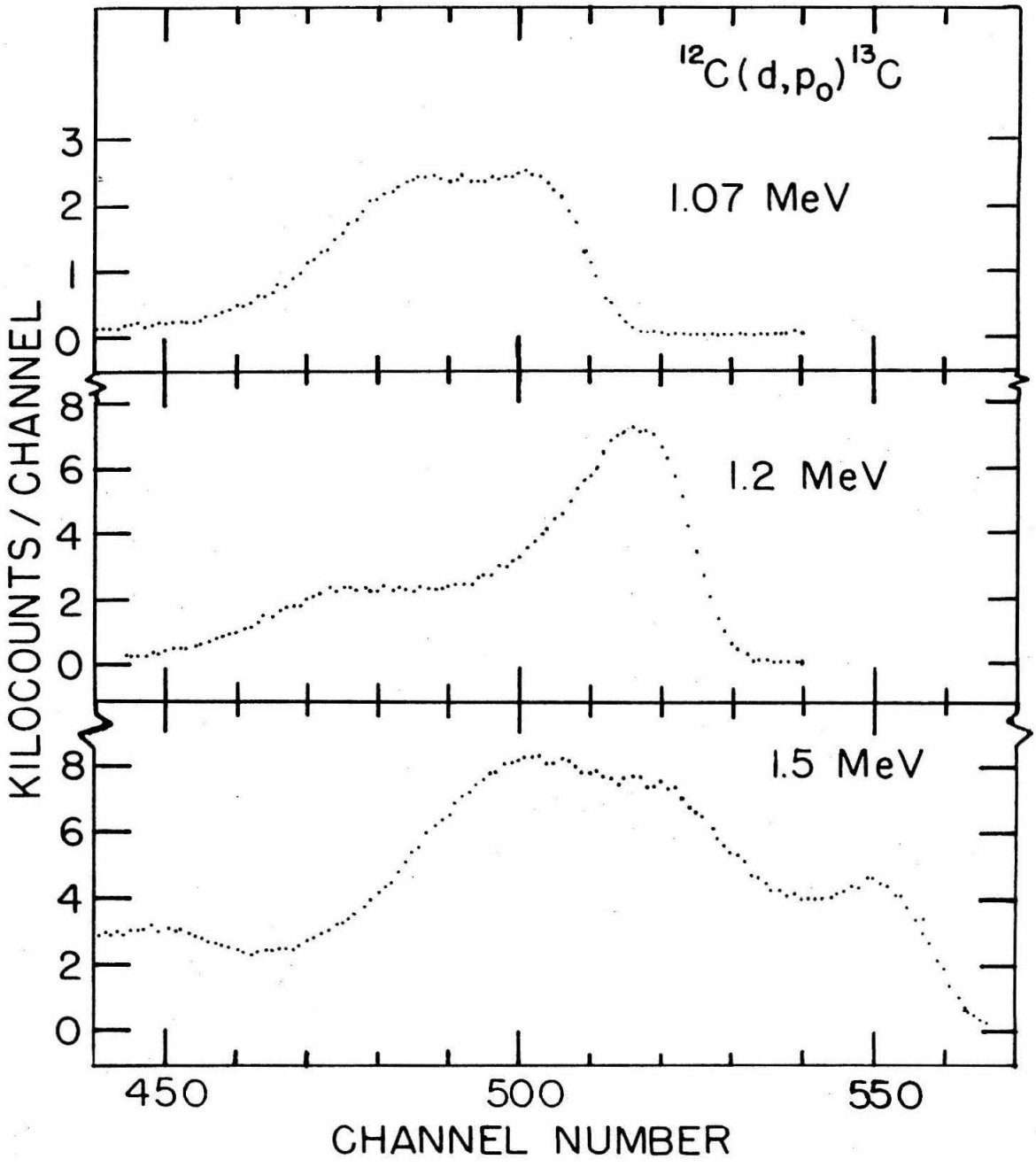
$^{12}C(d,p_0)^{13}C$
1.07 MeV
1.2 MeV
1.5 MeV
KILOCOUNTS/CHANNEL
CHANNEL NUMBER
450
500
550

Figure 4

FIGURE 5

Schematic drawing of energy dependence of detected protons at $\theta_{lab} = 160°$ for the reaction $^{12}C(d,p_0)^{13}C$. Proton 4 energy is shown to depend on deuteron energy loss, proton energy loss, and kinematic factors. (See text, page 10.)

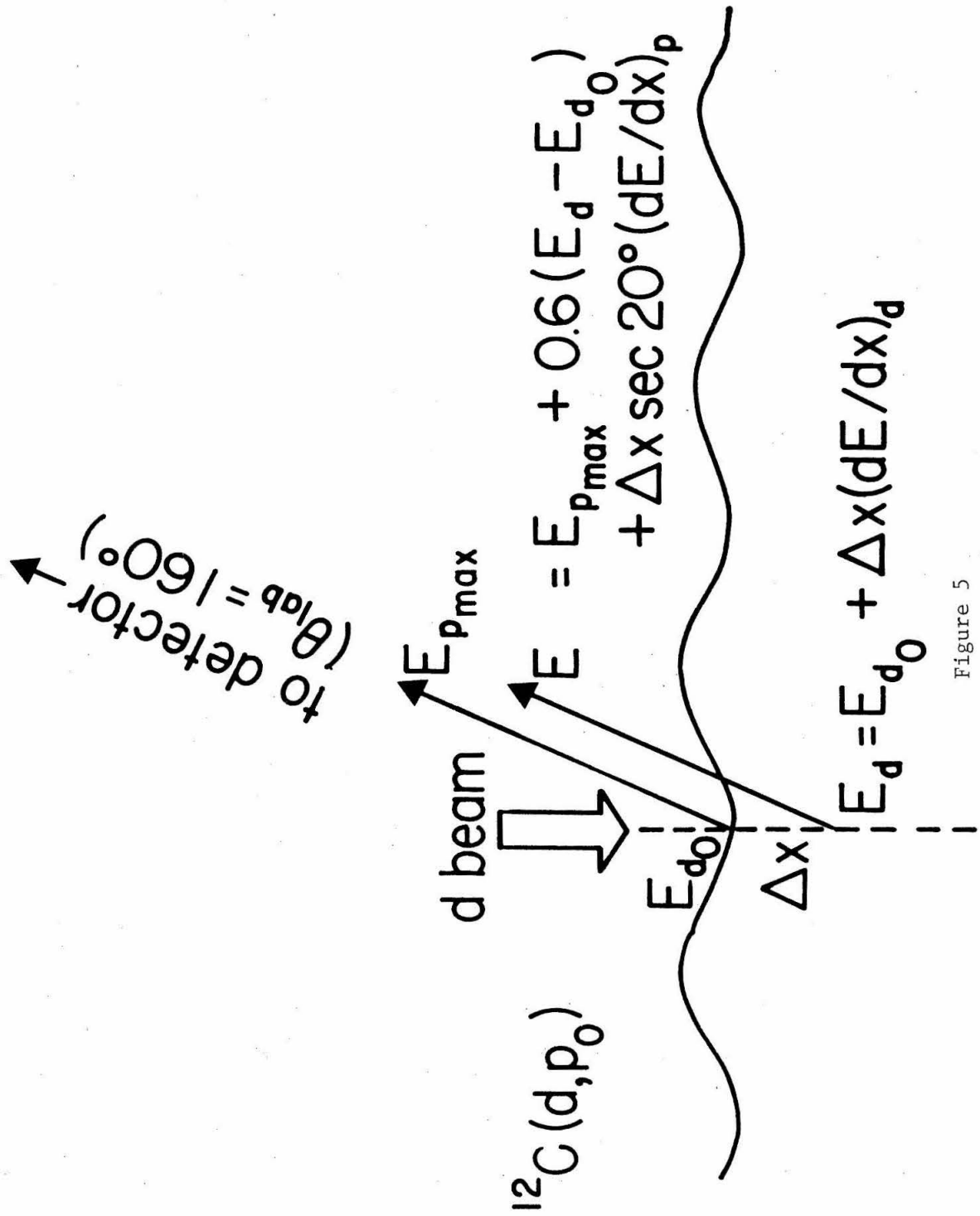
to detector
($\theta_{lab} = 160°$)
$E_{p_{max}}$
$E = E_{p_{max}} + 0.6(E_d - E_{d_0}) + \Delta x \sec 20° (dE/dx)_p$
d beam
$^{12}C(d,p_0)$
E_{d_0}
Δx
$E_d = E_{d_0} + \Delta x (dE/dx)_d$

Figure 5

FIGURE 6

Pulse height spectra for quartz glass and lunar exterior sample 64455,33 from $^{12}C(d,p_0)^{13}C$ reaction. Quartz glass was cleaned in perchloric acid and high purity distilled water. Sample 64455,33 has been exposed to solar wind while on the lunar surface, and was stored in a plastic conical vial in the dry nitrogen glove box for three years. Quartz glass is seen to have surface carbon only, while 64455,33 shows both surface and thick target yields. $^{12}C(d,p_0)$ peak is centered in channel 507; the higher energy proton group seen on quartz glass spectrum is a $^{28}Si(d,p)$ group. (See text, page 11.)

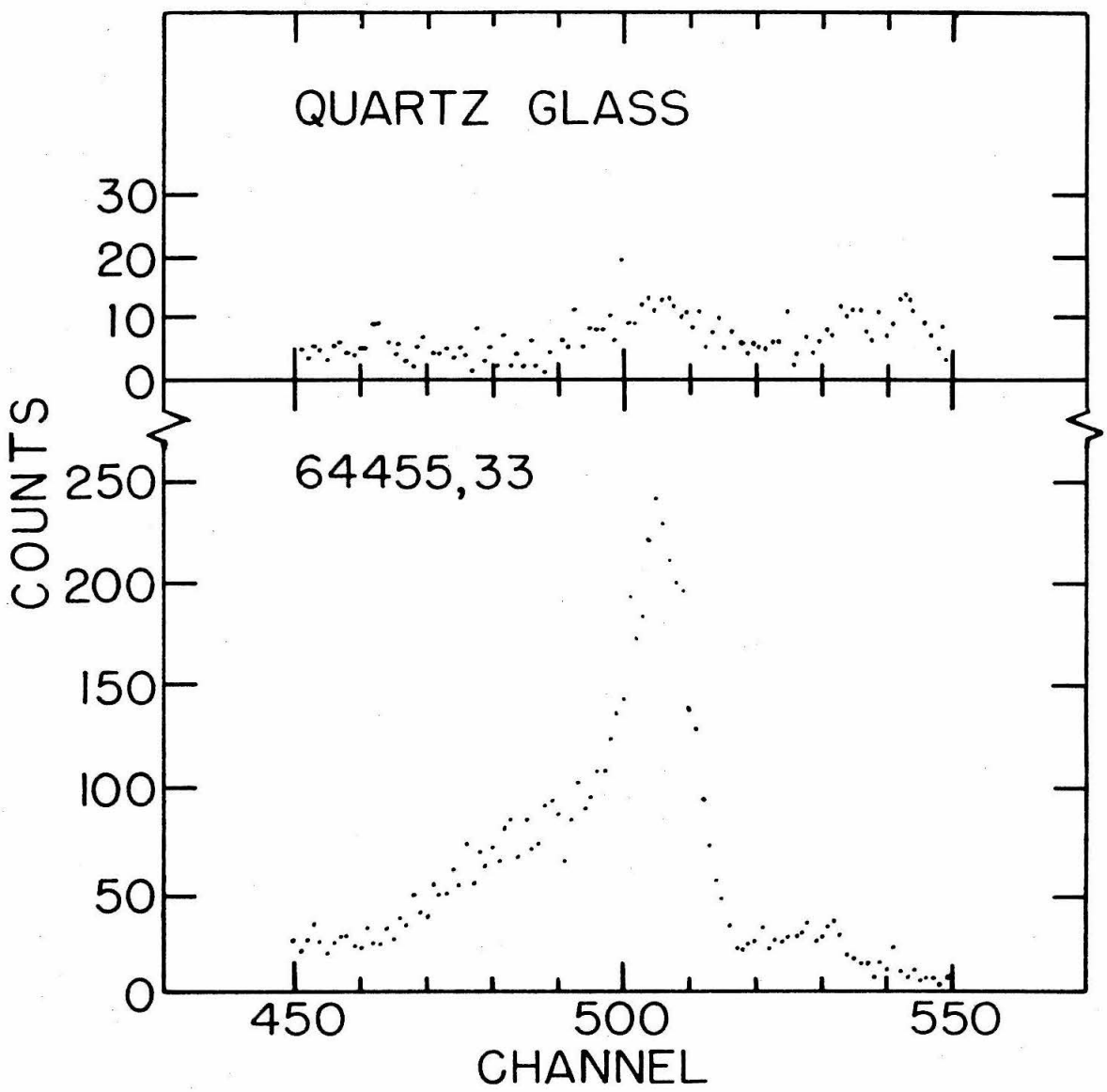
QUARTZ GLASS
30
20
10
0
64455,33
250
200
150
100
50
0
COUNTS
450
500
550
CHANNEL

Figure 6

FIGURE 7

Schematic drawing of the ultra-high vacuum target chamber, beam line vacuum system, and detectors used. Drawing is not to scale. NaI = sodium iodide gamma ray detector at 0° lab angle; PM = photo-multiplier tube; Si S B = silicon surface barrier detector at 160° lab angle. (See text, page 13.)

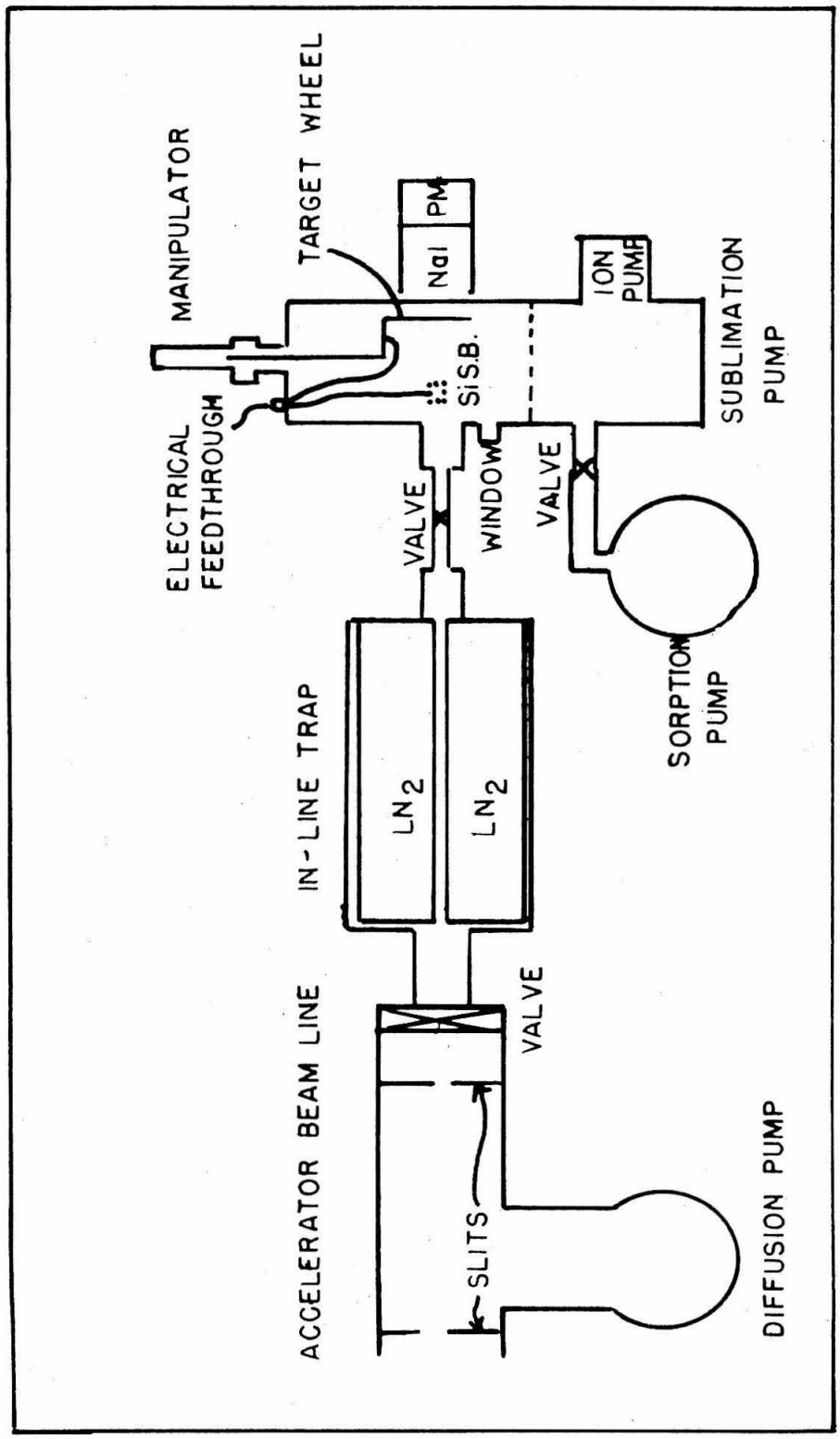
MANIPULATOR
TARGET WHEEL
NaI
PM
ION PUMP
ELECTRICAL FEEDTHROUGH
Si S.B.
SUBLIMATION PUMP
VALVE
WINDOW
VALVE
IN-LINE TRAP
LN2
LN2
SORPTION PUMP
ACCELERATOR BEAM LINE
VALVE
SLITS
DIFFUSION PUMP

Figure 7

FIGURE 8

Pulse height spectrum for 900 keV protons incident on 300 $\mu g/cm^2$ CaF_2 target for the reaction $^{19}F(p,\alpha\gamma)^{16}O$. Total integrated proton charge was 2 microcoulombs. The positions of full energy peaks for 6.13, 6.92, and 7.12 MeV gamma rays as detected by a 3"×3" NaI(Tl) crystal are indicated by FEP, FEP_2, and FEP_3. Corresponding single and double escape peaks are marked SEP, DEP, SEP_2, and SEP_3 (double escape peaks for two higher energy gamma rays fall under FEP_1). Spectrum includes portion of Compton scatter events in the crystal; limits of integration indicated include part of this Compton tail in addition to all gamma-ray peaks. Gamma ray energy vs. channel calibration is made using ^{88}Y source. (See text, page 15.)

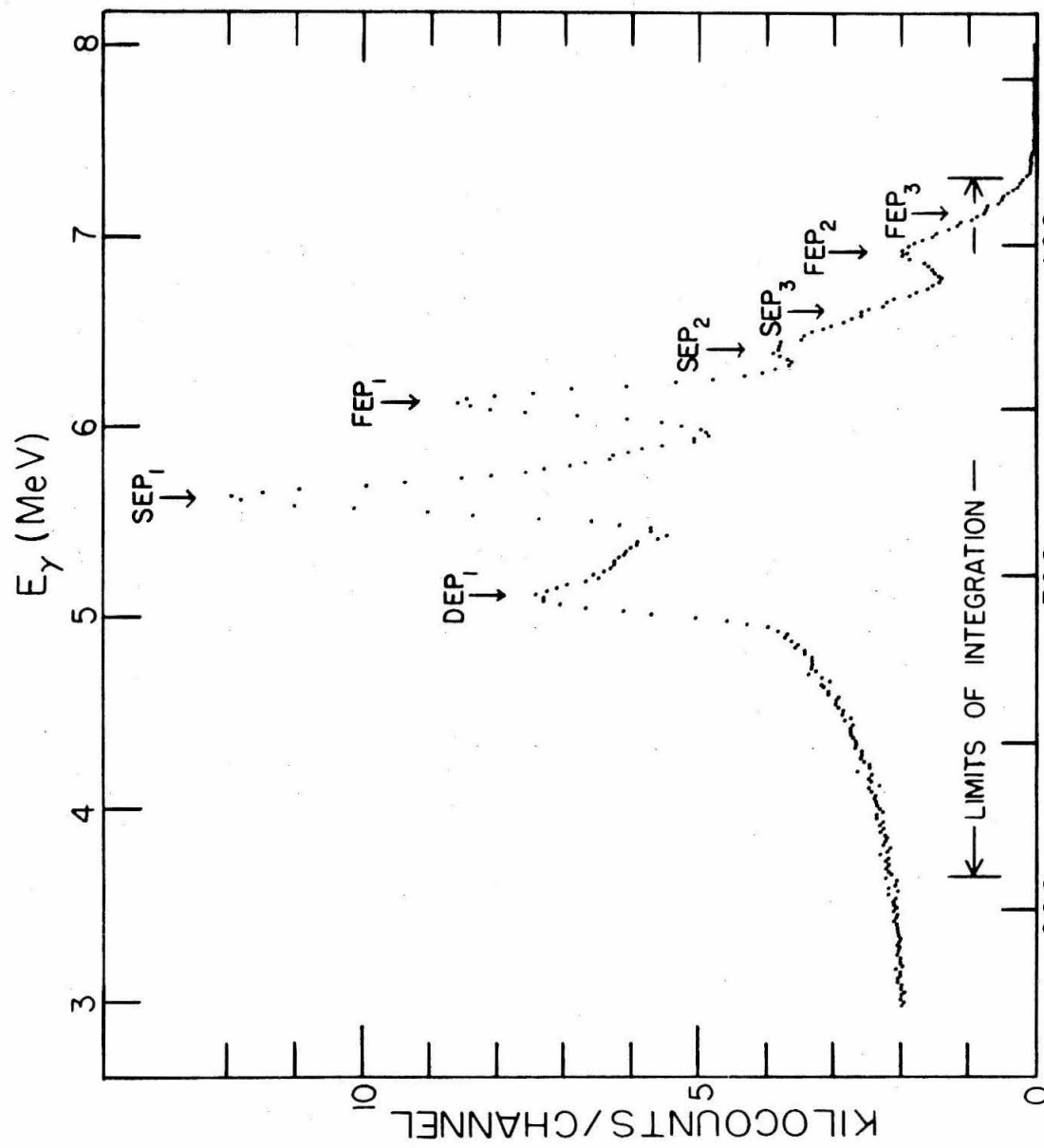
E_γ (MeV)
3
4
5
6
7
8
SEP$_1$
FEP$_1$
DEP$_1$
SEP$_2$
SEP$_3$
FEP$_2$
FEP$_3$
LIMITS OF INTEGRATION
200
300
400
CHANNEL
KILOCOUNTS/CHANNEL
0
5
10

Figure 8

FIGURE 9

Fluorine concentration versus depth profiles for two crushed samples of the Murchison carbonaceous chondrite. Increase in gamma ray yield at the resonance energy is seen. Error bars show typical statistical uncertainties. (See text, page 19.)

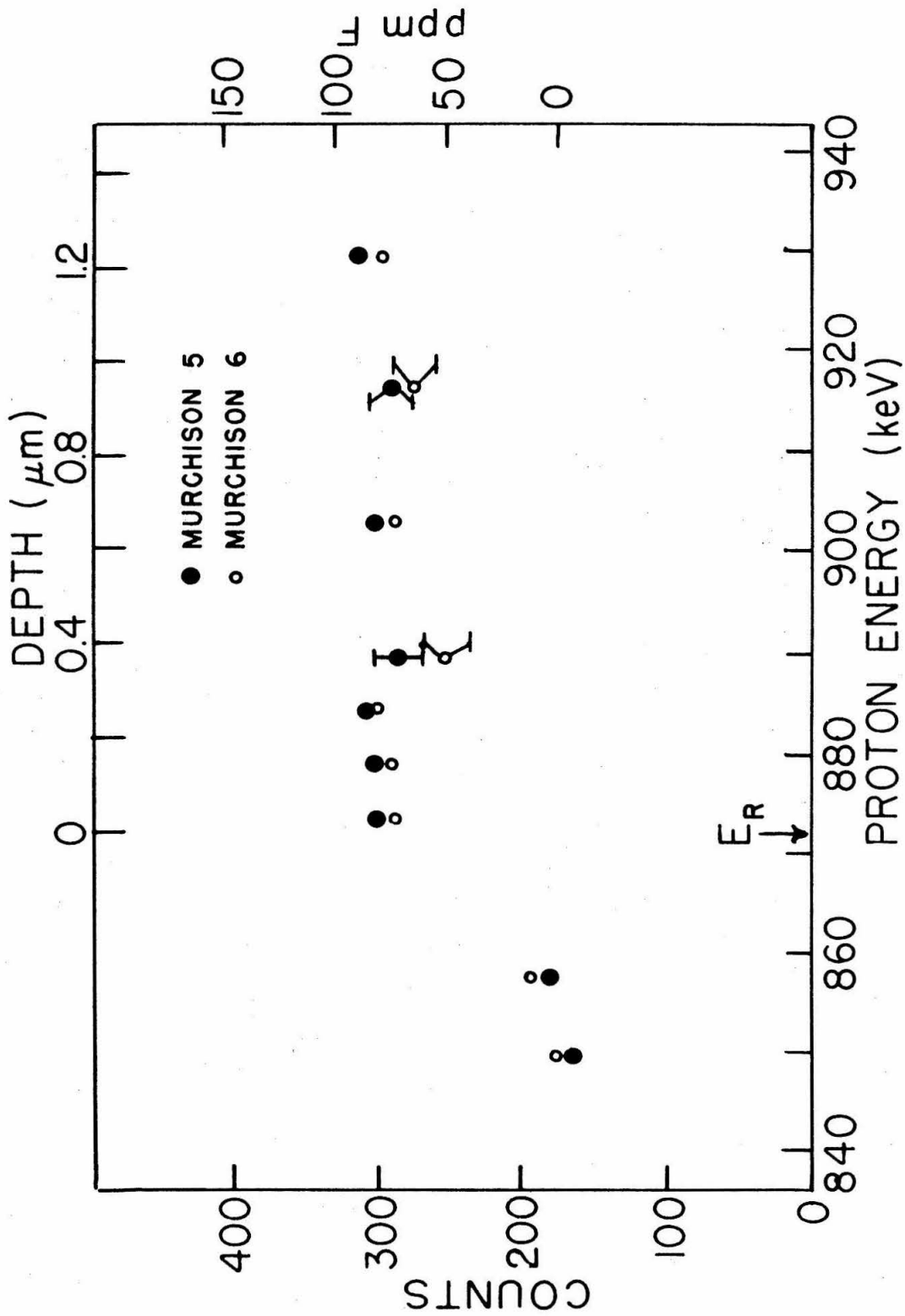
DEPTH (μm)
0
0.4
0.8
1.2
ppm
150
100
50
0
MURCHISON 5
MURCHISON 6
COUNTS
400
300
200
100
0
840
860
880
900
920
940
E_R
PROTON ENERGY (keV)

Figure 9

FIGURE 10

Top: Fluorine concentration versus depth for sample 70019,17, a sealed rock box sample. Exterior points are from measurements of a glass coating; interior points are from measurements of an interior soil breccia surface, freshly exposed in our laboratory (Leich et al., 1974).

Bottom: Fluorine concentration versus depth for anorthosite coarse fine 66044,8, and patinated breccia 75075,2, both sealed rock box samples. Shown are data from two surfaces of 66044,8, and from an interior surface freshly exposed in our laboratory. The smooth dashed curve is drawn through the data points of 75075,2 for clarity in the figure.

The depth scale has not been corrected for electrostatic charging of the samples, but the profiles shown are consistent with surface F peaks on all samples. (See text, page 23.)

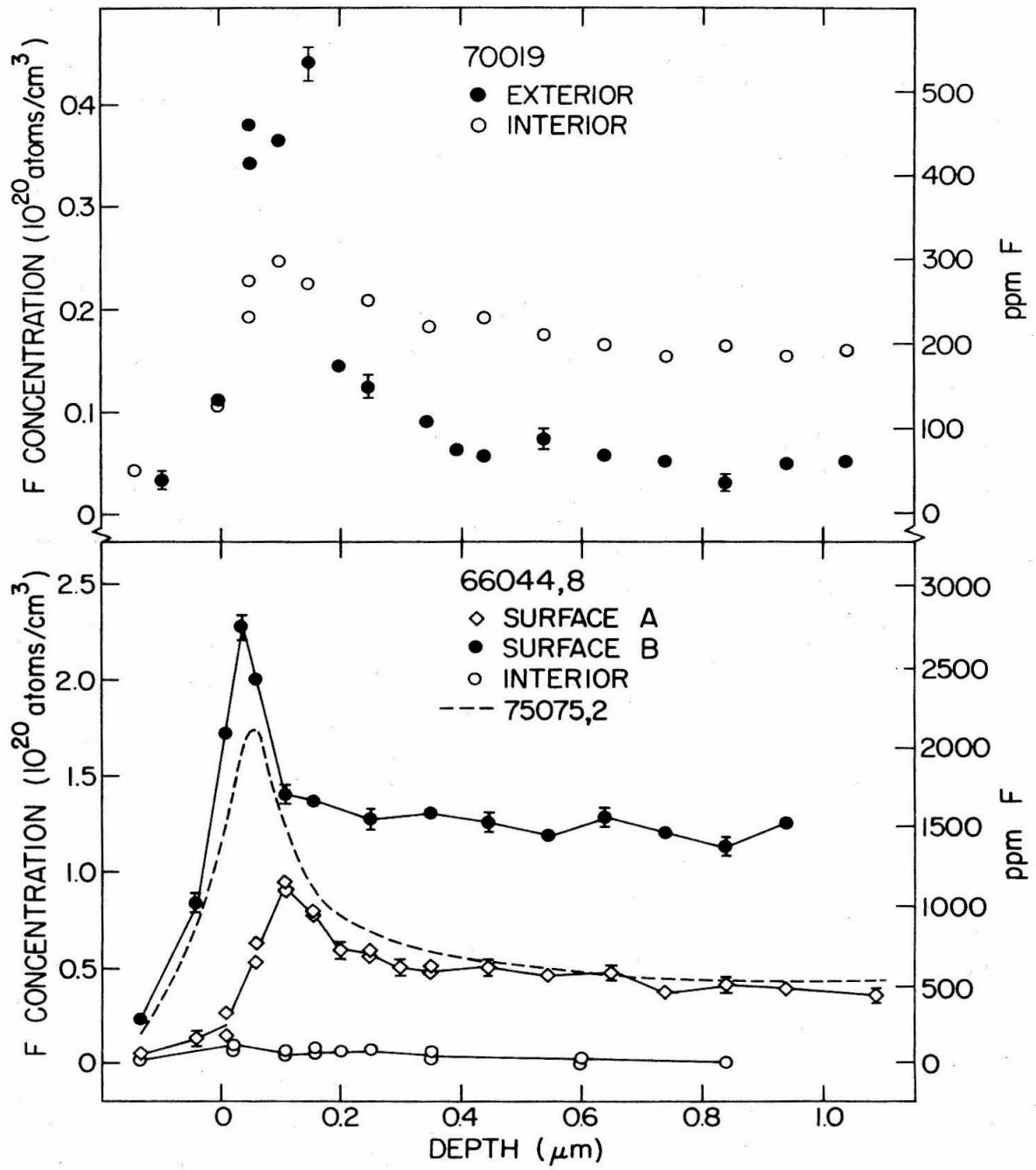
70019
EXTERIOR
INTERIOR
F CONCENTRATION (10^{20} atoms/cm^3)
ppm F
66044,8
SURFACE A
SURFACE B
INTERIOR
75075,2
DEPTH (μm)

Figure 10

FIGURE 11

Fluorine concentration versus depth for quartz glass discs. Solid points correspond to a disc packaged in Teflon by the Lunar Curatorial Facility; open points are data from a disc serving as a control. The depth of the peak location of F concentration is probably caused by electrostatic charging of the sample during proton beam bombardment. (See text, page 24.)

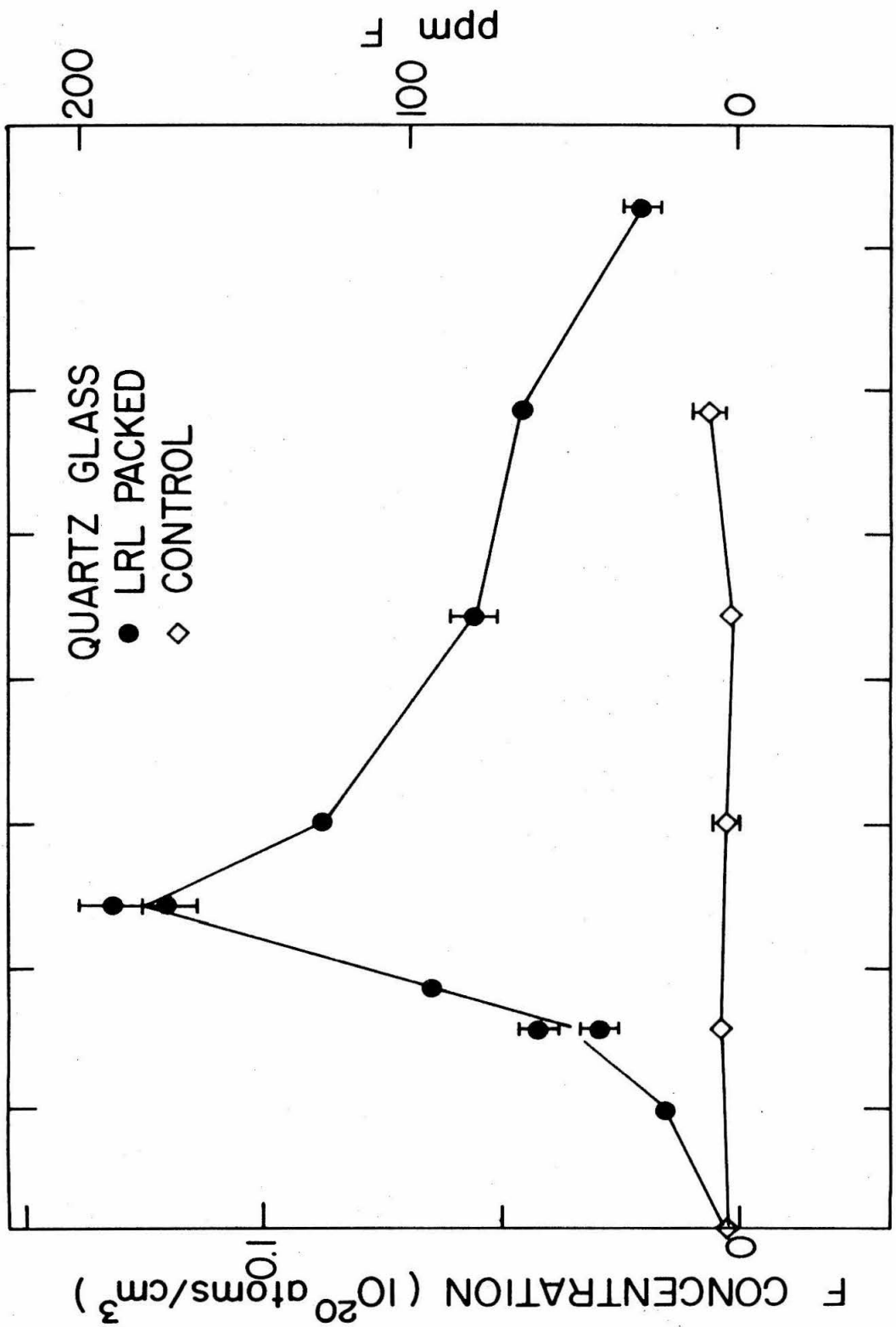
QUARTZ GLASS
● LRL PACKED
◇ CONTROL
F CONCENTRATION (10^{20} atoms/cm^3)
ppm F
DEPTH (μm)
0
0.2
0.4
0.6
0.8
1.0
1.2
100
200

Figure 11

FIGURE 12

Depth profiles of fluorine concentrations of two samples from rock 76215. A smooth dashed curve has been drawn through the data points for sample 76215,19, a projecting knob of rock 76215. The width of the distribution reflects uneven charging of the sample by the proton beam and is probably not a good indication of the depth to which fluorine is present (Goldberg et al., 1975). The depth scale has been corrected in an average sense by a shift in the beam energy of the $^{27}Al(p,\gamma)$ 992 keV resonance (Leich et al., 1974). The 76215,19 concentrations have been divided by ten to facilitate comparison to data from sample 76215,33. This sample is a crystalline-lined cavity (vug), for which no electrostatic charging correction was necessary. (See text, page 25.)

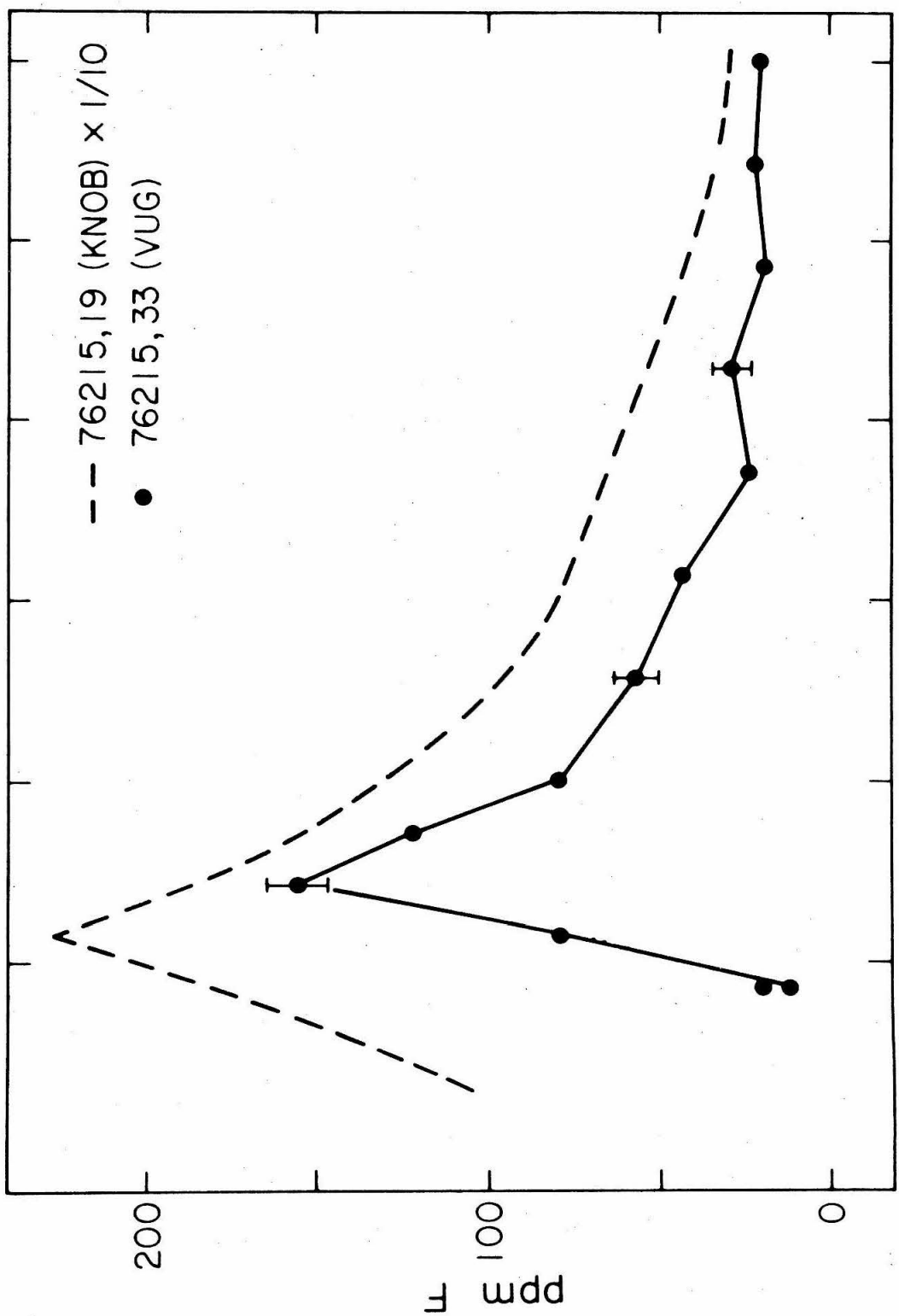
-- 76215,19 (KNOB) x 1/10
• 76215,33 (VUG)
ppm F
200
100
0
0
.2
.4
.6
.8
1.0
DEPTH (μm)

Figure 12

FIGURE 13

Depth profiles of fluorine concentration for two glass-coated soil breccia chips from sample 15012, an Apollo 15 Sealed Environment Surface Container (SESC) sample. The brown "glassy" surfaces (indicated by solid points) show a uniform distribution of fluorine consistent with bulk values of lunar fluorine concentrations. The significant surface peaks and distribution of fluorine with depth for the soil "breccia" surfaces are due to the presence of surface coatings on green glass spheres which are present in the breccia surface. The dashed line for the 15012,67 breccia surface profile is an average of interior data point values. (See text, page 27.)

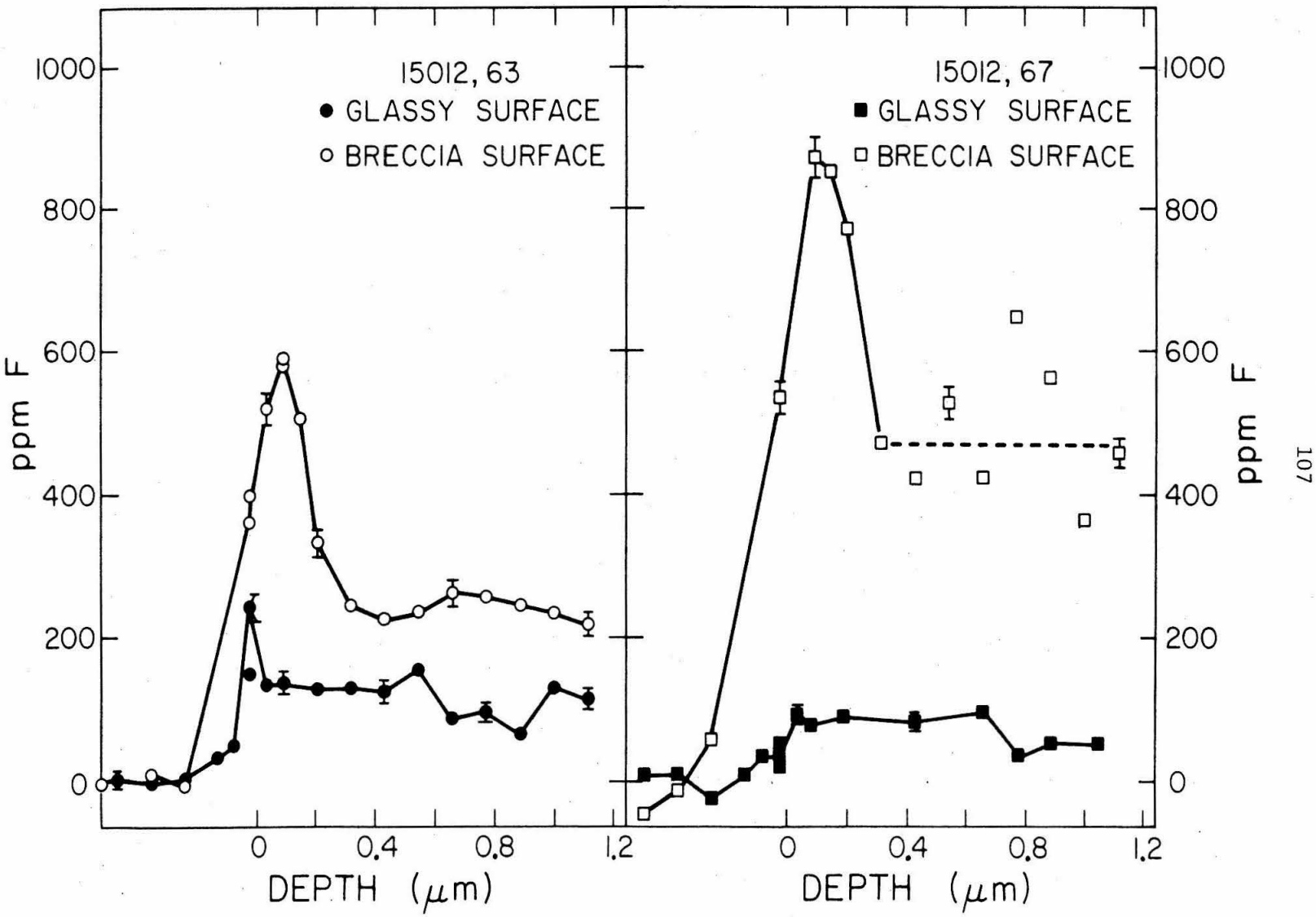
15012, 63
● GLASSY SURFACE
○ BRECCIA SURFACE
15012, 67
■ GLASSY SURFACE
□ BRECCIA SURFACE
ppm F
1000
800
600
400
200
0
0
0.4
0.8
1.2
DEPTH (μm)

Figure 13

FIGURE 14

Fluorine depth profiles for handpicked green glass separates from soil sample 15427,39. A profile of the fluorine content of the stainless steel screen behind which the samples were mounted is also shown. The "uncleaned green glass" is composed of transparent whole green spheres larger than 175 microns diameter. The "cleaned green glass, d > 175 m" is composed of primarily devitrified fragments (note that this concentration profile is divided by two). The "cleaned green glass, 100 μm < d < 175 μm" sample is a mixture of fragments, primarily transparent. Cleaning refers to an ultrasonic rinse in high-purity methanol. The data shown are consistent with thin (~ monolayer) surface films. (See text, page 31.)

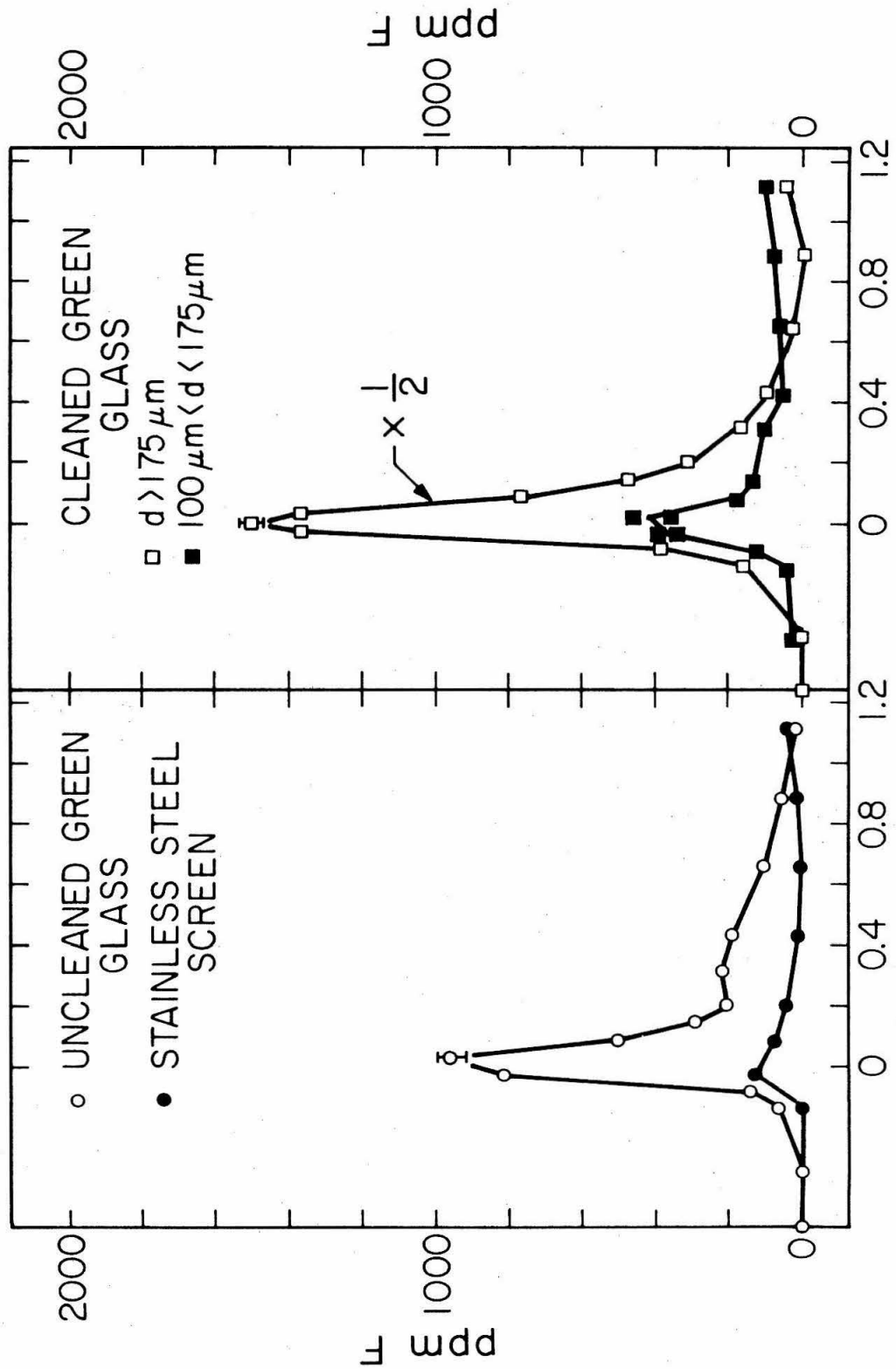
UNCLEANED GREEN GLASS
STAINLESS STEEL SCREEN
CLEANED GREEN GLASS
d > 175 μm
100 μm < d < 175 μm
× 1/2
ppm T
2000
1000
0
0.4
0.8
1.2
DEPTH (μm)

Figure 14

FIGURE 15

Fluorine concentration versus depth profiles for two samples from soil 15427,39. The closed data points ("green glass spheres") are from the sample of "uncleaned green glass" of Figure 14 after ultrasonic rinsing in high purity methanol. The concentration profile is divided by two so that the "brown fragments" fluorine concentration is more easily seen. The brown fragments have a uniform concentration of 67 ppm F, with no surface enhancement. (See text, page 31.)

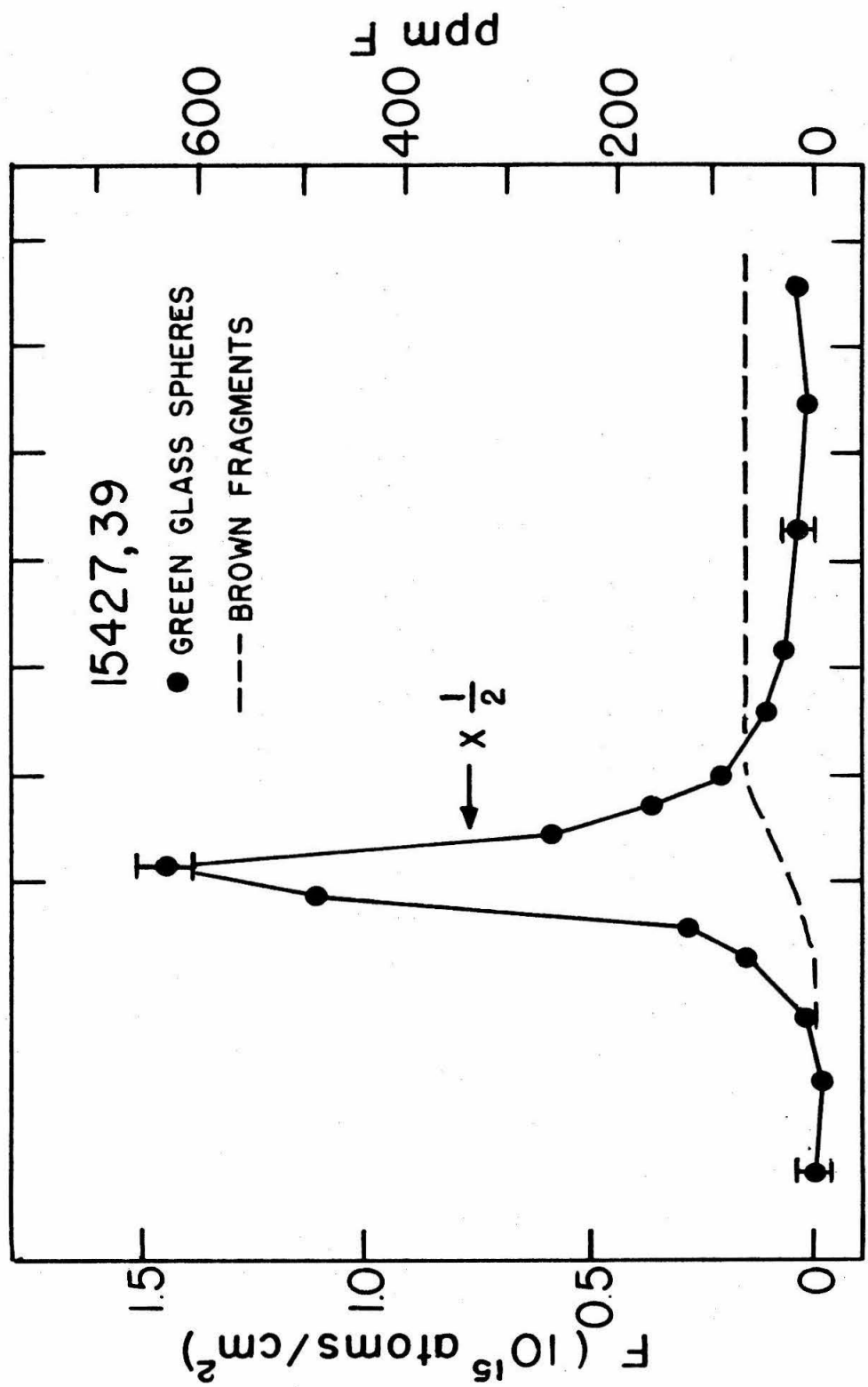
15427,39
GREEN GLASS SPHERES
BROWN FRAGMENTS
x 1/2
DEPTH (μm)
ppm T
T (10^15 atoms/cm^2)
0
0.4
0.8
1.2
200
400
600
0.5
1.0
1.5

Figure 15

FIGURE 16

Fluorine concentration versus depth for orange glass sample 74220,28. The sample contained a sizable fraction of partially broken orange glass spheres in addition to whole spheres. The sample was ultrasonically rinsed in high-purity methanol. (See text, page 37.)

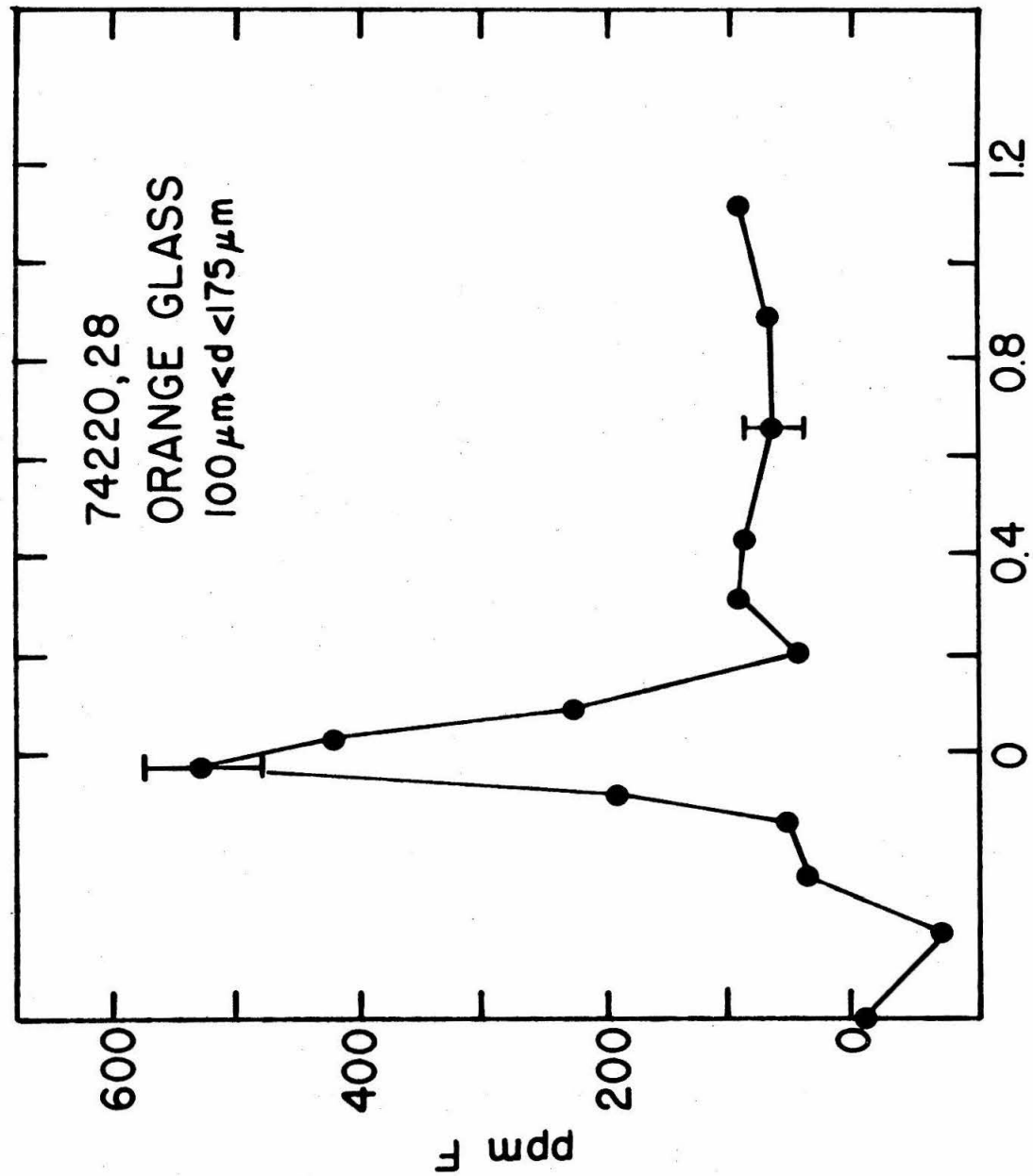
74220,28
ORANGE GLASS
100μm<d<175μm
ppm F
600
400
200
0
0
0.4
0.8
1.2
DEPTH (μm)

Figure 16

FIGURE 17

Fluorine concentration versus depth for orange soil 74220,235. This sample was composed of handpicked whole orange glass spheres, and ultrasonically rinsed in high-purity methanol. (See text, page 37.)

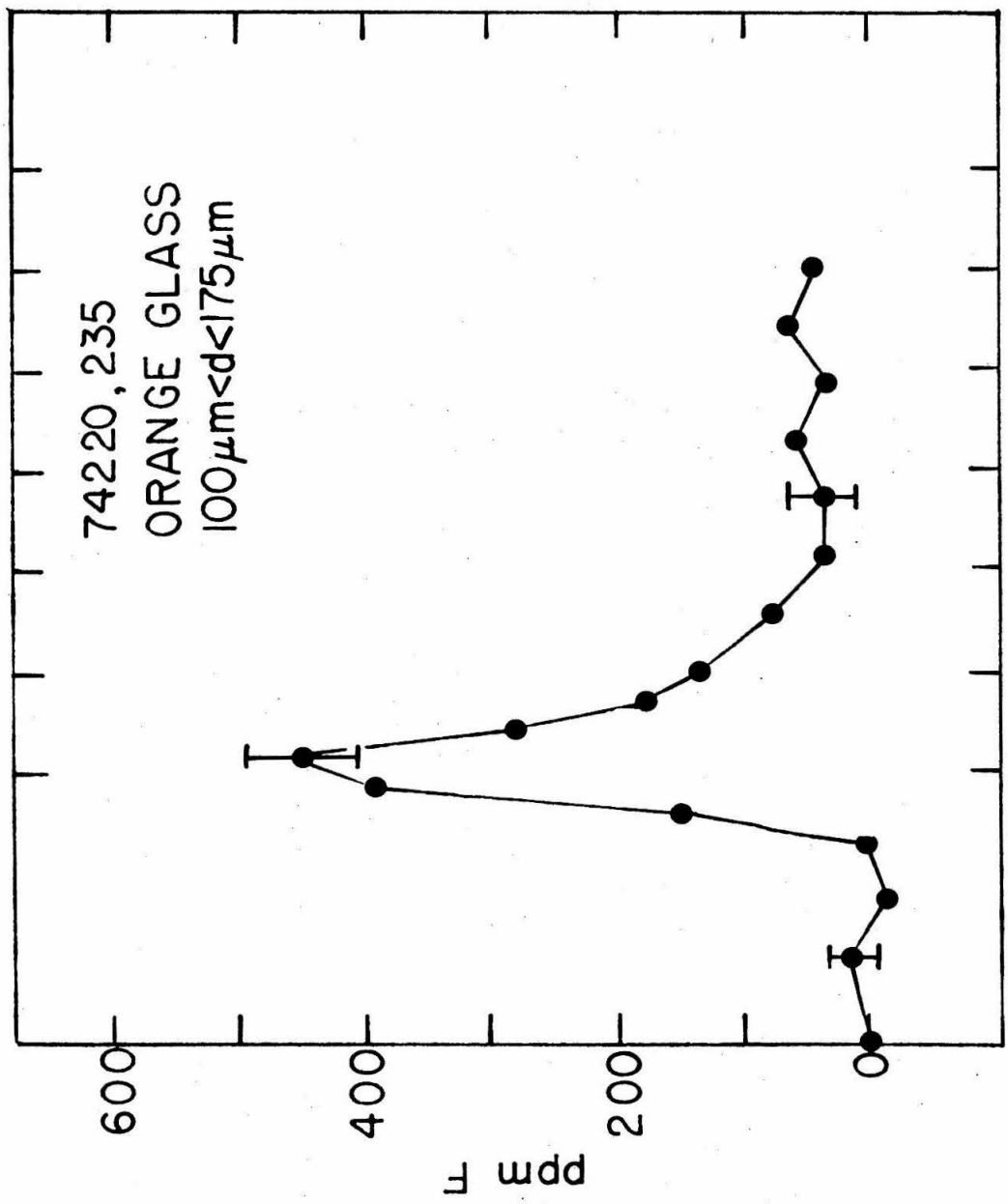
74220,235
ORANGE GLASS
100μm<d<175μm
ppm F
600
400
200
0
0
0.4
0.8
1.2
DEPTH (μm)

Figure 17

FIGURE 18

Fluorine concentration versus depth profiles for three 74220 samples. Solid lines connect data points for two samples of 74220,174: a > 100 μm sizing of handpicked unbroken orange glass spheres and spheroids (data shown with triangles) and a > 100 μm sizing of the residue after the handpicking process (data shown with solid circles) which contained broken orange glass fragments. The "basalt fragments" (taken from 74220,235) data are shown by a dashed curve for simplicity in the figure; an average volume concentration of 95 ppm F is obtained. These profiles have been corrected for packing efficiency. (See text, page 37.)

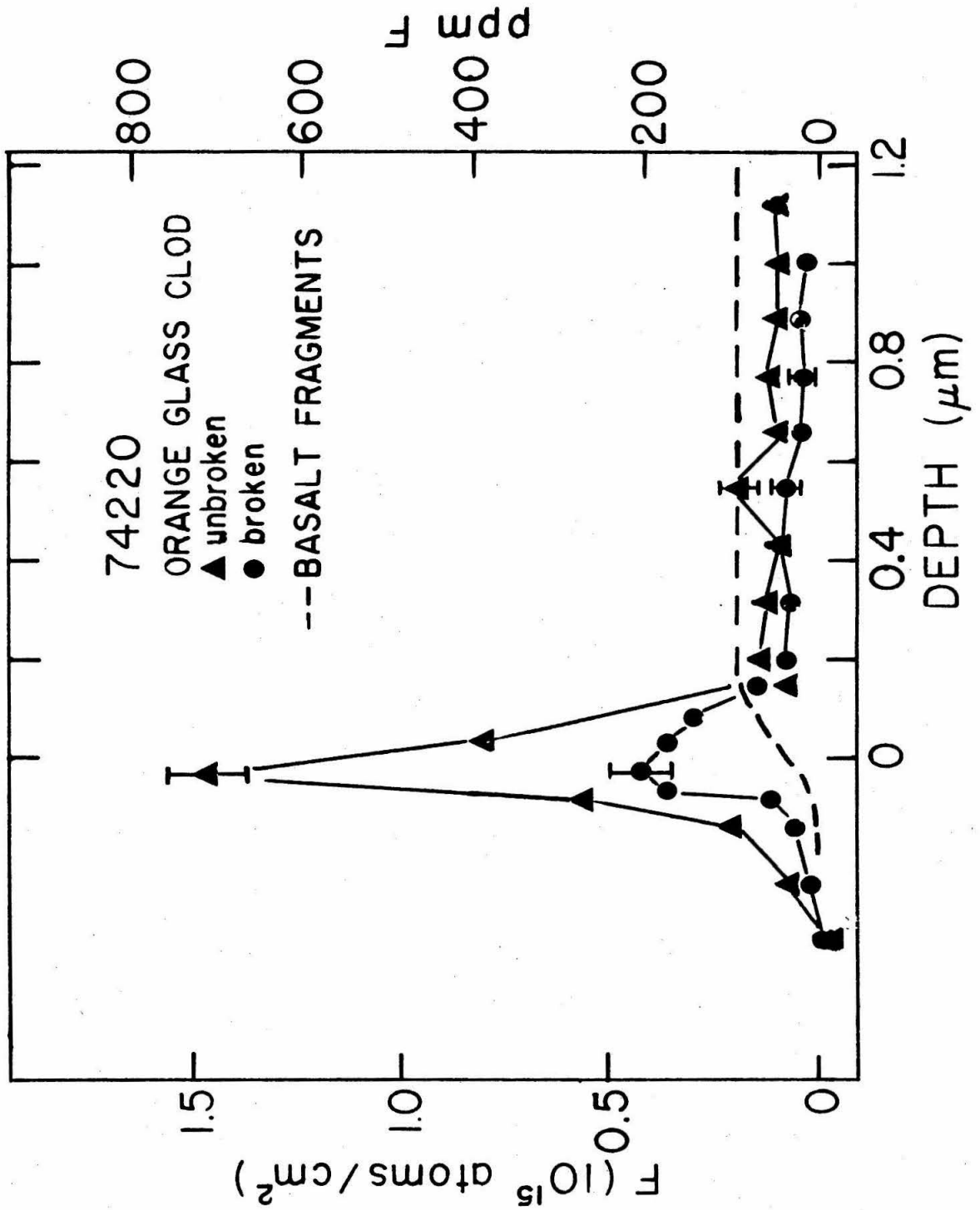
74220
ORANGE GLASS CLOD
▲ unbroken
● broken
--BASALT FRAGMENTS
F (10^{15} atoms/cm^2)
ppm F
DEPTH (μm)
0
0.5
1.0
1.5
200
400
600
800
0.4
0.8
1.2

Figure 18

FIGURE 19

Fluorine concentration versus depth profiles for two vesicles from basalt 15556,94. Both show a surface enhancement of F with uniform concentrations at greater depths. (See text, page 42.)

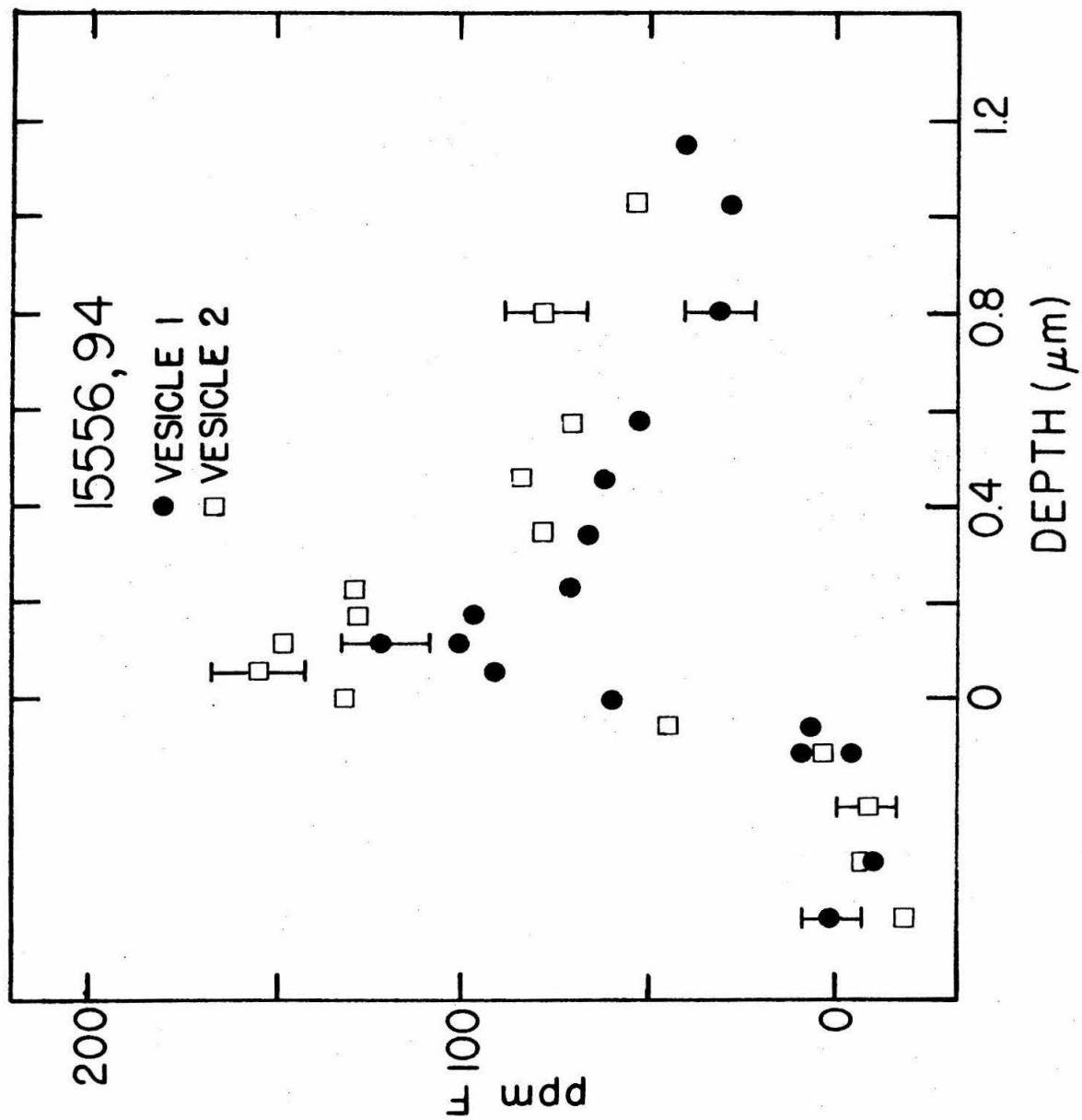

Figure 19

FIGURE 20

Fluorine concentration versus depth profile for a sawed surface of basalt 15556,94 which contained no vesicles. No surface enhancement of F is seen, and the interior concentration is similar to that of 15556,94 vesicles (Figure 19). (See text, page 42.)

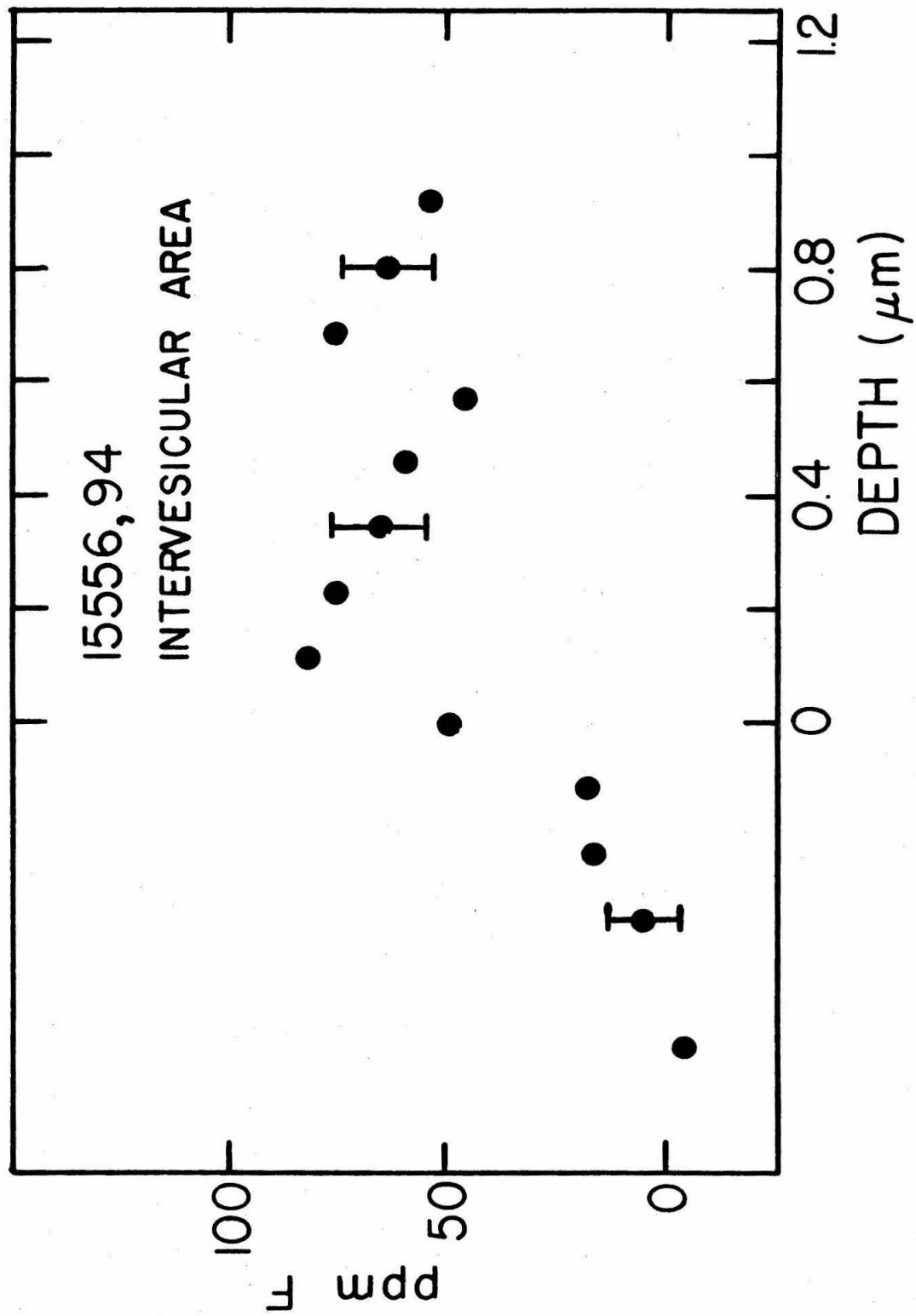

Figure 20

FIGURE 21

Fluorine concentration versus depth profiles for two samples from basalt 15016,176. The open data points are taken for a freshly exposed vesicle lining, the closed points for an intervesicular area. Surface enhancement of F is seen for the vesicle only. (See text, page 42.)

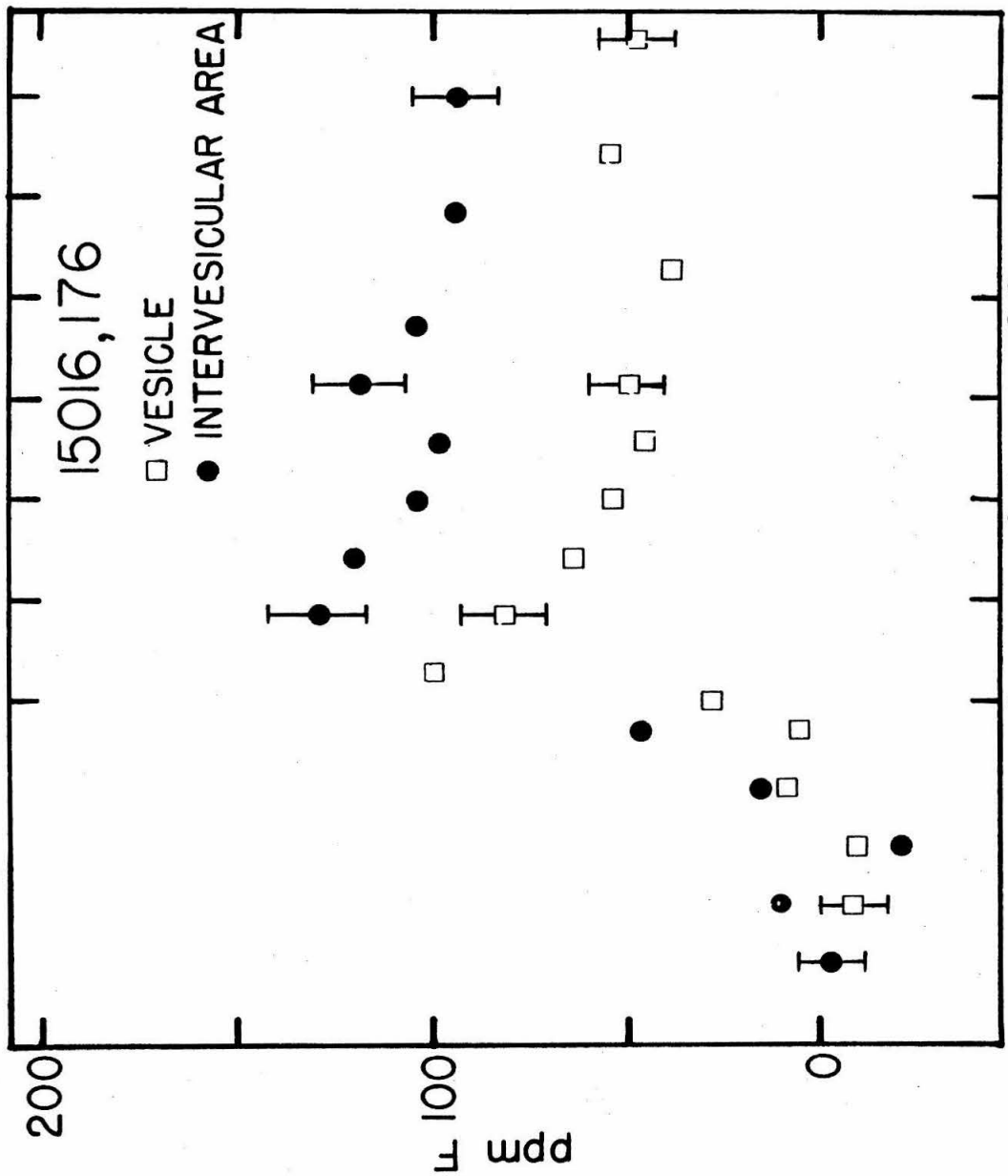
15016,176
□ VESICLE
● INTERVESICULAR AREA
200
100
0
ppm T
0
0.4
0.8
1.2
DEPTH (μm)

Figure 21

FIGURE 22

Fluorine depth profiles for silica glass discs dipped in 0.5% HF solution for the times indicated. The discs were then rinsed in H_2O and methanol. The F measured was stable during proton beam bombardment and appears to be tightly fixed to the glass. The unshown 10 second dip profile is essentially identical to the 1 second profile. (See text, page 48.)

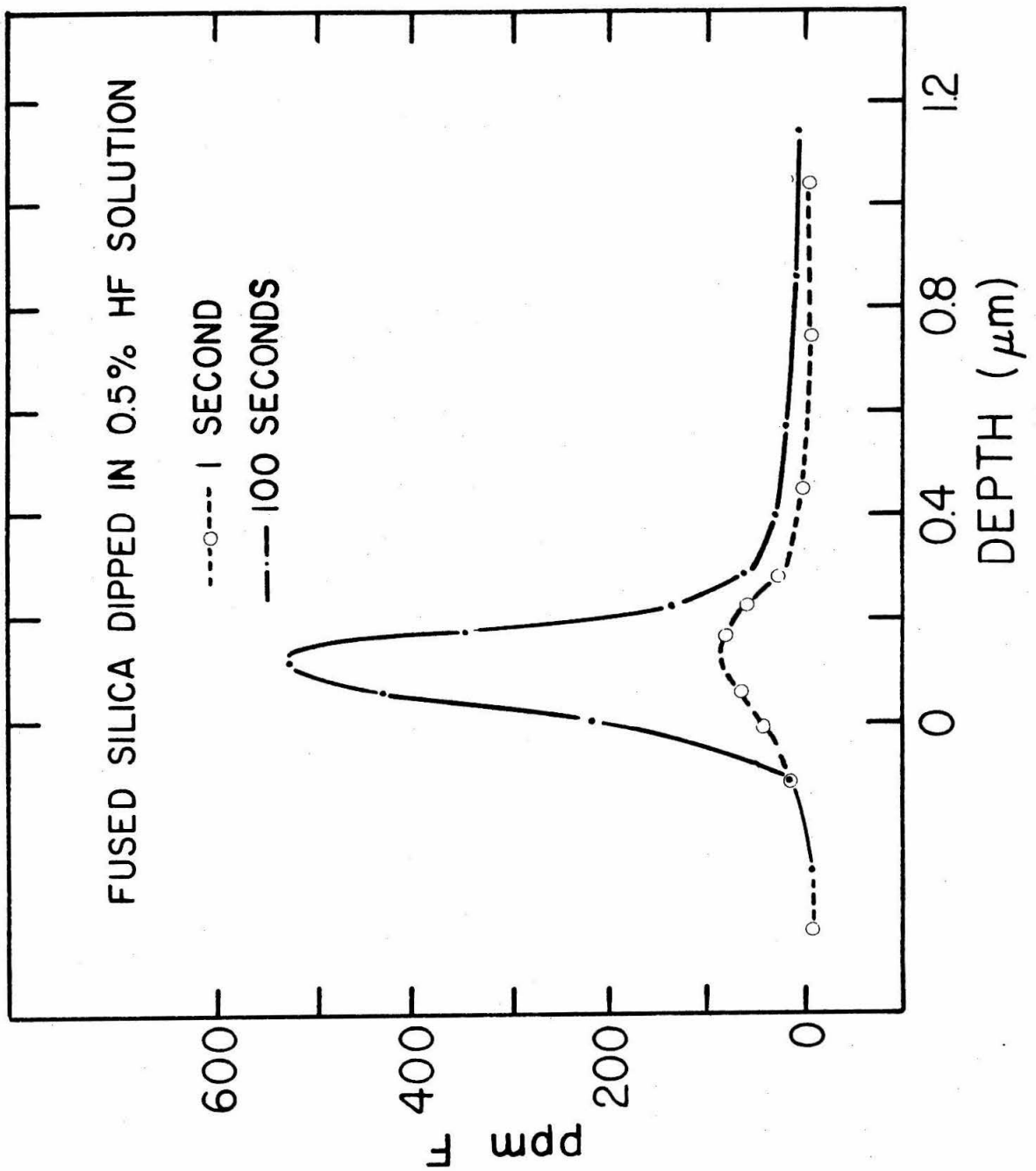
FUSED SILICA DIPPED IN 0.5% HF SOLUTION
---○--- 1 SECOND
—·— 100 SECONDS
ppm F
600
400
200
0
0
0.4
0.8
1.2
DEPTH (μm)

Figure 22

FIGURE 23

Particle spectrum taken at 1.20 MeV deuteron bombardment energy, showing $^{16}O(d,p_1)$, $^{16}O(d,p_0)$, and $^{12}C(d,p_0)$ groups for a thin carbon film on a quartz backing. ^{16}O content of green and orange glasses is evaluated by integrating counts over both groups, and comparing to silica glass spectrum. (See text, page 66.)

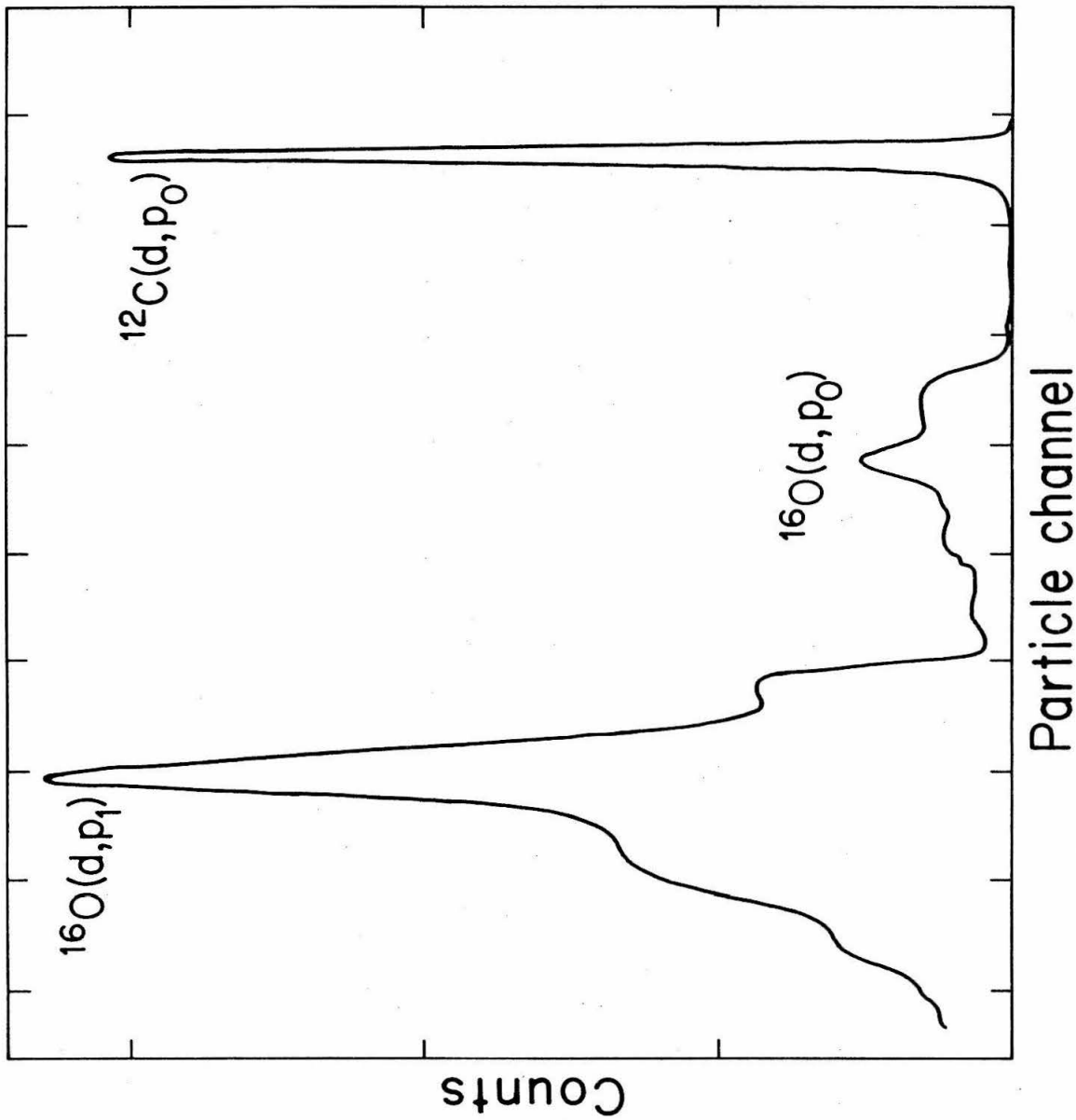

Figure 23